Experimental investigation and Machine Learning-based prediction and optimization of mechanical properties of Biochar-Enhanced High-Strength concrete

Experimental Investigation and Machine Learning-Based Prediction and Optimization of Mechanical Properties of Biochar-Enhanced High-Strength Concrete

sustainability

MDPI

Article

Experimental Investigation and Machine Learning-Based Prediction and Optimization of Mechanical Properties of Biochar-Enhanced High-Strength Concrete

Shah Room *, Ali Bahadori-Jahromi, Marwah Al Tekreeti and Zeeshan Tariq

Department of Civil Engineering and Built Environment, School of Computing and Engineering, University of West London, London W5 5RF, UK; ali.bahadori-jahromi@uwl.ac.uk (A.B.-J.); marwah.altekreeti@uwl.ac.uk (M.A.T.); zeeshan.tariq@uwl.ac.uk (Z.T.)

* Correspondence: shah.room@uwl.ac.uk

Abstract

Biochar has emerged as a sustainable additive in concrete production, offering potential for improved concrete performance and waste valorization. An experimental investigation was conducted using wood waste biochar as a partial cement replacement at 0%, 2%, 4%, and 6% by weight. Compressive strength (CS) and split tensile strength (STS) were determined at 7 and 28 days, while flexural strength (FS) was determined at 28 days. The experimental results demonstrated that 2 to 4% biochar replacement enhanced CS by 9.67% and FS by 15.40%, while STS showed optimal improvement at 2% replacement by 6.24%. To extend these findings across diverse feedstocks and mix designs, a comprehensive database of 318 mixes incorporating 13 biochar types was compiled from literature to develop machine learning (ML) models for predicting all three strength properties simultaneously. Random Forest (RF) and Gradient Boosting (GBR) algorithms were optimized using nested 5-fold cross-validation and compared against a Ridge regression baseline. The optimized RF model (n_estimators = 1000) achieved a nested cross-validated R^2 of 0.817 $\pm$ 0.072 and a 32.5% reduction in RMSE compared to the baseline, with testing R^2 values of 0.894 for CS, 0.828 for FS, and 0.537 for STS. (SHapley Additive exPlanations) (SHAP) analysis identified cement content, coarse aggregate (CA) content, and biochar dosage as the most influential features. Biochar effect curves, based on the most reliable datasets (rice husk, n = 69; wood, n = 52), demonstrated that rice husk biochar consistently enhanced all three strength properties, while wood biochar showed superior performance for FS and STS. Experimental validation using wood waste biochar confirmed that model predictions closely matched measured strengths, with 90% prediction intervals reliably encompassing experimental values. The developed models offer a practical decision-support tool for sustainable concrete mix design, significantly reducing experimental effort while providing evidence-based guidance for biochar feedstock selection and dosage optimization, keeping the cement usage at a minimum.

Keywords: biochar-concrete; machine learning; random forest; compressive strength; flexural strength; split tensile strength; SHAP analysis; sustainable construction materials

Academic Editor: Muhammad Junaid Munir

Received: 5 April 2026
Revised: 8 May 2026
Accepted: 15 May 2026
Published: 18 May 2026

1. Introduction

Cement is the primary binder material used in concrete and is responsible for approximately 8% of global CO_2 emissions, with each ton of cement production releasing 0.85 to 0.92 tons of CO_2 [1,2]. Global cement production exceeds around 4 billion tons per

annum, which urges an urgent need to explore sustainable alternatives and supplementary cementitious materials that reduce the environmental footprint of concrete production [3,4]. The global construction sector is responsible for about 40% of global energy-related CO_2 emissions, making the shift towards green construction materials a top priority for the mitigation of climate change [5]. Supplementary cementitious materials such as silica fume, fly ash, slag, and natural pozzolans have been significantly studied as partial replacement of cement, offering both green benefits and improved performance of the concrete [6]. Similarly, a carbon-rich material, biochar produced through pyrolysis of biomass under hypoxic or anoxic conditions, has recently gained attention as a novel additive in cement-based composites [7].

In the UK, around 10.1 million tons of roundwood were used in 2024, generating substantial amounts of wood waste during processing. Alongside, the generation of wood waste is about 5 million tons annually from construction, demolition, furniture manufacturing, and packaging sectors [8]. Of this, around 1.5 million tons of wood waste is sent to landfill or incineration, indicating an extensive loss of valuable biomass resources. Currently, the domestic capacity of biochar production in the UK is estimated to be more than 1 million tons annually [9]. The UK biochar market is quickly developing, supported by initiatives such as the UK Biochar Research Center, which promotes sustainable production and application of biochar in various sectors, including construction. The UK government's devotion to attaining net-zero carbon emissions by 2050 has accelerated interest in innovative waste valorization plans, including the conversion of waste wood into biochar [10]. These statistics confirm a viable feedstock supply chain for sourcing biochar from wood waste, supporting its integration as a sustainable additive in biochar-enhanced concrete formulations. Biochar is derived from numerous feedstocks, including agricultural waste, forestry residues, and municipal solid waste, which offer multiple benefits to the cement-based composites, including carbon sequestration through carbon storage in concrete, enhanced mechanical performance mainly through filler and internal curing effects, improved durability through pore refinement, and sustainable waste management [11].

The use of high-strength concrete plays an important role in modern construction due to its improved performance; however, the high use of cement in its production poses a challenge to sustainable construction. Therefore, it is important to explore the incorporation of biochar in high-strength concrete to optimize the mix proportions by limiting the use of cement. A study reported that the addition of 2 to 4% biochar as partial replacement of cement by weight increased the 28-day CS of high-strength mortar by 20%, attributed to enhanced hydration and internal curing effects [12]. A study conducted on high-strength concrete incorporated with wood biochar reported durability improvement by microstructure refinement of the concrete [13,14]. The high specific surface area of biochar provides nucleation sites for hydration products, accelerating early-age strength development [15]. Due to the porous nature of biochar, it can reduce workability and increase water demand, leading to careful adjustment of water and use of SP [16]. Excessive biochar content, widely reported as more than 5% by weight of cement, can adversely affect the performance of the cement-based composites [7]. The optimization of biochar dosage is therefore critical for achieving the desired strength class while maintaining workability and durability [17]. The tendency of biochar to limit the use of cement in high-strength concrete can be optimally utilized due to the high demand for cement in the production of high-strength concrete. The high-strength concrete optimal mix design remains a complex and time-consuming process, especially when using alternative materials, often relying on trial mix experimental work.

ML methods have appeared as influential tools for predicting various concrete characteristics, capturing complex non-linear relationships between mix ingredients and per-

formance characteristics [18,19]. Various algorithms, including GBR, RF, artificial neural networks (ANN), support vector machines (SVM), and gene expression programming (GEP), have been successfully applied to predict various strength parameters of conventional and blended cement concretes [20–22]. Recent studies have shown the advantage of ensemble methods, particularly RF and GBR, for concrete characteristics prediction due to their ability to resist overfitting through ensemble averaging, handle non-linearity and provide feature importance rankings [23,24]. Table 1 presents the evidence of ML methods successfully used for concrete mechanical properties predictions.

Table 1. Application of various ML models for the successful prediction of concrete mechanical properties.

ML Model	Strength Characteristics	Evaluation Indices	Key Findings	References
ANN	CS	R^2, RMSE	High accuracy in strength prediction with R^2 values of up to 0.98 for CS	[25–27]
	FS	R^2, RMSE	Strong predictive performance achieved through data-driven approaches	[27]
	STS	R^2	ANN models demonstrated high prediction capability, enhancing the material properties of concrete	[27]
RF	CS	R^2, MSE, MAE	Effective at predicting mechanical strength with less sensitivity to overfitting	[28]
	STS	R^2, RMSE, MAE	High accuracy, aiding in sustainable concrete development with waste materials	[29]
	FS	R^2, RMSE, MAE	High accuracy in strength prediction with R^2 values of up to 0.91	[30]
Extreme Gradient Boosting (XGBoost)	CS	R^2, RMSE	Outperformed traditional methods, achieving R^2 values above 0.98 in CS predictions	[31]
	FS	R^2	Proven effectiveness in predicting the strength properties of various mixes	[31]
SVM	STS	R^2, MAE	Enhanced prediction capabilities with robust performance indicators	[29,32]
Decision Trees (DT)	STS	R^2	Simple model capable of providing insights into influential factors in tensile strength	[29]
GBR	CS	R^2, RMSE	Improved accuracy in strength prediction compared to conventional methods	[27]
AdaBoost	STS	R^2, MSE, RMSE	Strong performance when combined with physics-based approaches, enhancing predictive robustness	[32]

Despite the predictive accuracy of ML models, their "black-box" nature has limited adaptation in materials science, where understanding the underlying mechanisms is as important as prediction accuracy [18]. Recent advances in model interpretability, particularly SHAP and partial dependence plots, have addressed this limitation by providing insights into feature importance and the relationships between input and output parameters [19,30]. These techniques have been increasingly applied in construction materials research to

validate model behavior against physical understanding and to extract actionable understandings [23,24,33].

1.1. Research Gap

Wood waste–derived biochar produced via pyrolysis at 500 °C, with a maximum particle size below 75 µm, was incorporated as a partial cement replacement at dosages of 2%, 4%, and 6% in high-strength concrete, aiming to evaluate its influence on both fresh and mechanical properties while contributing to waste valorization and carbon reduction strategies in the construction sector. The experimental program investigates fresh properties, including slump, density, and air content, alongside mechanical performance characterized by CS and STS at 7 and 28 days, and FS at 28 days. Another aim is to develop ML-based models for predicting mechanical properties and optimizing mix design. Despite the increasing application of ML in concrete research, several gaps remain. Existing studies rarely provide simultaneous prediction of CS, FS and STS for biochar-modified concrete. In addition, the effect of different biochar feedstocks has not been systematically incorporated into predictive frameworks. Furthermore, uncertainty quantification, particularly through prediction intervals, is often neglected, limiting the reliability of model outputs. Finally, practical tools for ML-driven mix design optimization are still lacking. This study addresses these limitations by integrating experimental data with advanced ML techniques to enable accurate prediction, uncertainty assessment, and practical optimization of biochar-incorporated high-strength concrete.

1.2. Research Objectives

This study addresses the identified gaps through the following objectives:

1. To conduct an experimental investigation on high-strength concrete incorporating wood waste biochar (pyrolyzed at 500 °C, particle size < 75 µm, at 2%, 4%, and 6% cement replacement), assessing both fresh and mechanical properties.
2. To develop a comprehensive dataset of diverse biochar types from literature and experimental results from the wood waste biochar.
3. To develop and evaluate multi-output ML models, including RF and GBR, for the simultaneous prediction of CS, FS, and STS, and benchmark them against a baseline Ridge regression using nested cross-validation to ensure robustness and generalizability.
4. To assess the influence of different biochar types from various feedstocks on CS, FS, and STS of concrete using a ML model for the optimal content of each type of biochar.
5. To enhance interpretability and practical application by applying SHAP analysis to identify key input parameters and interactions, quantile regression to quantify prediction uncertainty, and a multi-objective (Pareto-based) optimization framework to translate predictions into sustainable mix design guidance.

2. Materials and Methods

2.1. Experimental Program

2.1.1. Materials

Ordinary Portland cement (CEM I 52.5 N) conforming to BS EN 197-1:2011 [34], procured from Heidelberg Materials, Maidenhead, UK, was used as the primary binder. Coarse grit sand procured from Travis Perkins, London, UK, size 4 mm and below, with 2.65 specific gravity was used as FA, while river crushed stone with a nominal maximum size of 10 mm and a specific gravity of 2.75 retained on sieve size 4 mm was used as CA, both conforming to BS EN 12620:2013 [35]. The fine and CA had a moisture content of 1.35% and 1.02%, respectively. The aggregates used to produce concrete mixtures were from the same batch and were oven dried at a temperature of 100 ± 5 °C for 24 h and

cooled down at room temperature to ensure the uniformity of all the mixtures. Figure 1 shows the biochar, CA and FA used in this research work. Physical properties of the FA, CA, biochar and superplasticizer (SP) used in this research work are given in Table 2.

(**a**) (**b**) (**c**)

Figure 1. (**a**) Wood waste biochar; (**b**) CA; (**c**) FA.

Table 2. Physical properties of the materials.

Description	Size (mm)	Specific Gravity/Bulk Density (g/cm^3)	Water Absorption (%)
Biochar	<0.075	0.41 g/cm^3	-
CA	4–10	2.75	1.02
FA	0–4	2.65	1.35
SP	-	1.06	-

Wood mass-derived biochar sourced from Onnu Biochar, Maidenhead, UK was used in this research work as a partial replacement of cement. The biochar was obtained through pyrolysis at a furnace temperature of 500 °C and has a bulk density of 0.41 g/cm^3. The maximum particle size of the biochar was about 50 mm. The stock biochar contained 4.23% of moisture and was oven-dried at 100 ± 5 °C for 24 h and cooled down at room temperature for 6 h prior to grinding. The dried biochar was ground using a heavy-duty grinder and sieved through a sieve with a size of 75 µm to ensure a maximum particle size of below 75 µm. After sieving, the biochar was stored in airtight containers until its use in the production of concrete to avoid any moisture absorption due to its porous structure. The hydrophilic nature of the biochar reduces the workability of the concrete mixture, for which the modified polycarboxylate-based SP BS EN 934-2:2019 [36], procured from Sika Chemicals, Welwyn Garden City, UK, was used at a dosage of 1% of the total binder weight to ensure the required consistency of all the mixes. Normal tap water was used for the preparation and curing of concrete mixes.

2.1.2. Mix Design and Casting

High-strength concrete of average 28-day compressive strength of 55 MPa was selected as the control mix for this study in accordance with the specification requirements defined in BS 8500-1 [37] and proportioned according to the mix design procedures in BS 8500-2 [38]. The mix design details are given in Table 3. In the nomenclature, the letter "BC" represents biochar-modified concrete mix, followed by a number which represents the amount of biochar added in the mix as a partial replacement of cement. Biochar was added at 0%, 2%, 4%, and 6% by weight of cement. The mix proportion was designed to achieve a target workability of a consistence class S2 (50–90 mm slump) as per BS EN 206-1 [39]. All mixes were prepared with an effective constant water to cementitious ratio (w/cm) of 0.43. Due to the porous structure of the biochar SP, at a rate of 1% of the total binder weight was used in the mixes with biochar and 0.75% in the control mix to ensure the required consistency of all the mixes [40]. The concrete materials were added to a pan mixer in a dry state and

mixed for 30 s, followed by the addition of water and SP and the mixing was done until all the ingredients were mixed thoroughly to the required state. A concrete vibrating table was used to ensure the uniform compaction of all the mixes during casting, and was completed within 45 min after mixing. Specimens were demolded after 24 ± 2 h and water cured at room temperature until the day of testing.

Table 3. Concrete mix design.

Mix Type	BC (wt%)	Cement (kg/m^3)	BC (kg/m^3)	CA (kg/m^3)	FA (kg/m^3)	Water (kg/m^3)	Effective w/cm	SP (kg/m^3)
BC0	0	453.91	0.00	981.97	750.78	213.34	0.43	3.40
BC2	2	444.83	9.08	981.97	750.78	213.34	0.43	4.53
BC4	4	435.75	18.16	981.97	750.78	213.34	0.43	4.53
BC6	6	426.68	27.23	981.97	750.78	213.34	0.43	4.53

2.1.3. Fresh and Hardened Concrete Experimental Tests

Workability of the concrete mixes was measured through slump tests in accordance with BS EN 12350-2 [41], and density of the fresh concrete was obtained by the average of three tests for each concrete mix according to EN 12350-6 [42]. Air content of the concrete was computed through the standard method in accordance with ASTM C138/C138M-24a [43].

For the CS, FS and STS tests, three specimens were tested, and the average of the three tested samples was reported as the concrete strength. For CS, 100 mm cubes were tested at 7 and 28 days after moist curing, confirming to BS EN 12390-3:2019 [44]. The specimens were tested using a 3000 kN compression testing machine at a loading rate of 6 kN/s. STS was determined as per BS EN 12390-6:2023 [45] on 100 mm diameter × 200 mm cylinders at 7 and 28 days with a loading rate of 1.6 kN/s. FS was determined on prisms (100 × 100 × 500 mm) with a span length of 400 mm and loading rate of 0.2 kN/s at 28 days using two-point loading according to BS EN 12390-5:2019 [46]. The experimental setup is given in Figure 2.

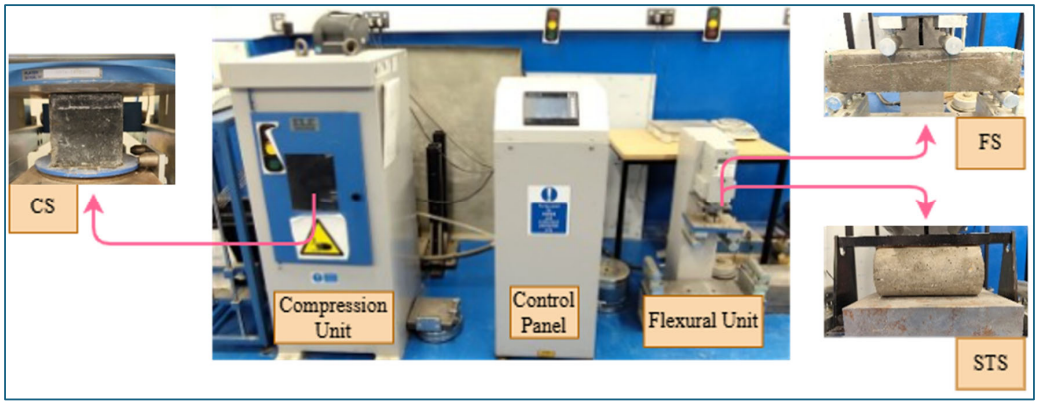

Figure 2. Experimental setup.

2.2. ML Modeling

ML techniques are used in this study to predict CS, FS and STS of biochar-enhanced concrete mixtures using the dataset from the literature and compared with the experimental results obtained from the tests performed. The research methodology framework is given in Figure 3.

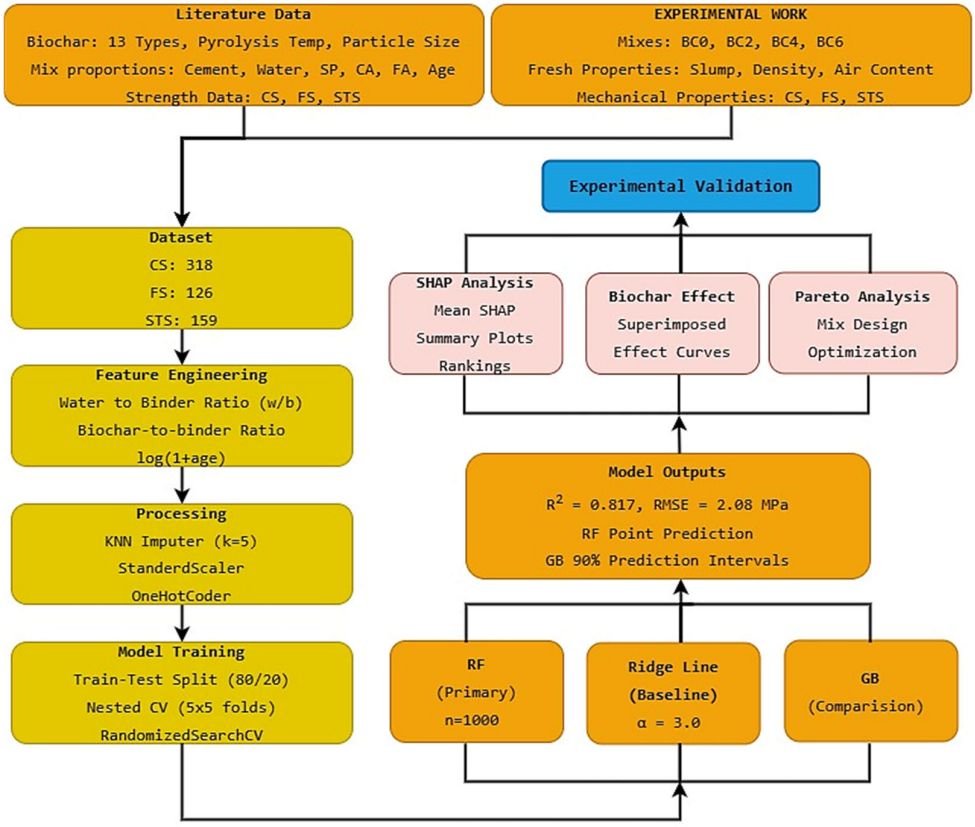

Figure 3. Research methodology framework.

2.2.1. Data Preprocessing and Feature Engineering

To enhance the diversity and robustness of the database, additional experimental data were compiled from published literature. This supplementary dataset included 13 biochar types: Rice Husk [15,17,47–50], Wood [15,16,51–53], Pine nut shell [14], Bamboo [54,55], Coffee grounds [56], Rice straw [57,58], Olive pits [51], Poultry litter [17], Pulp and paper [17], Soybean dregs [59], Carya cathayensis [60], and Municipal Solid Waste (MSW) [61]. The dataset was imported from an Excel workbook and cleaned by standardizing column names and casting numerical fields to numeric types. The complete experimental database comprised 318 samples, with CS data available for all 318 samples, while FS and STS were available for 126 and 159 samples, respectively. The statistical characteristics of the dataset are presented in Table 4.

A total of 13 input features were used for model development, categorized into numerical, categorical, and engineered features. The nine numerical features included cement content (kg/m^3), water content (kg/m^3), SP dosage (kg/m^3), CA content (kg/m^3), FA content (kg/m^3), biochar amount (kg/m^3), biochar particle size (μm), pyrolysis temperature (°C), and curing age (days). The categorical feature was biochar type, with 13 categories as listed above. Based on concrete materials science principles, three engineered variables were introduced: the water-to-binder ratio (w/b), calculated as water divided by the sum of cement and biochar; the biochar-to-binder ratio (biochar amount divided by cement plus biochar); and log-transformed curing age (log(1 + age)), which captures the non-linear strength development over time.

Table 4. Statistical summary of the dataset.

Parameter	Unit	n	Min	Max	Mean	Median	Std. Dev
Input Features							
Biochar amount	kg/m^3	318	0.0	129.9	19.7	13.5	22.5
Biochar Max particle size	µm	225	0.0	4000.0	366.7	50.0	903.8
Pyrolysis temperature (PT)	°C	279	0.0	700.0	448.9	500.0	207.8
Cement	kg/m^3	318	248.5	520.0	400.0	401.6	58.3
Water	kg/m^3	318	60.0	225.0	166.3	180.0	40.4
SP	kg/m^3	318	0.0	15.0	1.6	0.0	3.0
CA (CA)	kg/m^3	318	673.3	1221.0	1076.7	1122.0	108.7
FA	kg/m^3	318	375.5	915.0	695.2	700.5	117.1
Age	days	318	3.0	90.0	20.1	28.0	13.7
w/b ratio	-	316	0.115	0.785	0.424	0.436	0.113
Biochar-to-binder ratio	-	316	0.000	0.429	0.052	0.031	0.070
Output Targets							
CS	MPa	318	10.3	93.3	39.4	37.0	16.2
FS	MPa	126	1.8	8.2	4.9	4.9	1.4
STS	MPa	159	1.5	6.5	3.3	3.3	0.9

All preprocessing steps were implemented within a scikit-learn Pipeline and ColumnTransformer framework to ensure reproducibility and prevent data leakage. Missing values in numeric features were imputed using a K-nearest neighbors imputer (KNNImputer, k = 5). The missingness map is given in Figure 4. Numeric variables were standardized using StandardScaler to ensure that features with different units and scales contribute equally to model training [62]. The categorical biochar variable was encoded using one-hot encoding (OneHotEncoder with unknown-category handling), creating binary indicator variables for each biochar type.

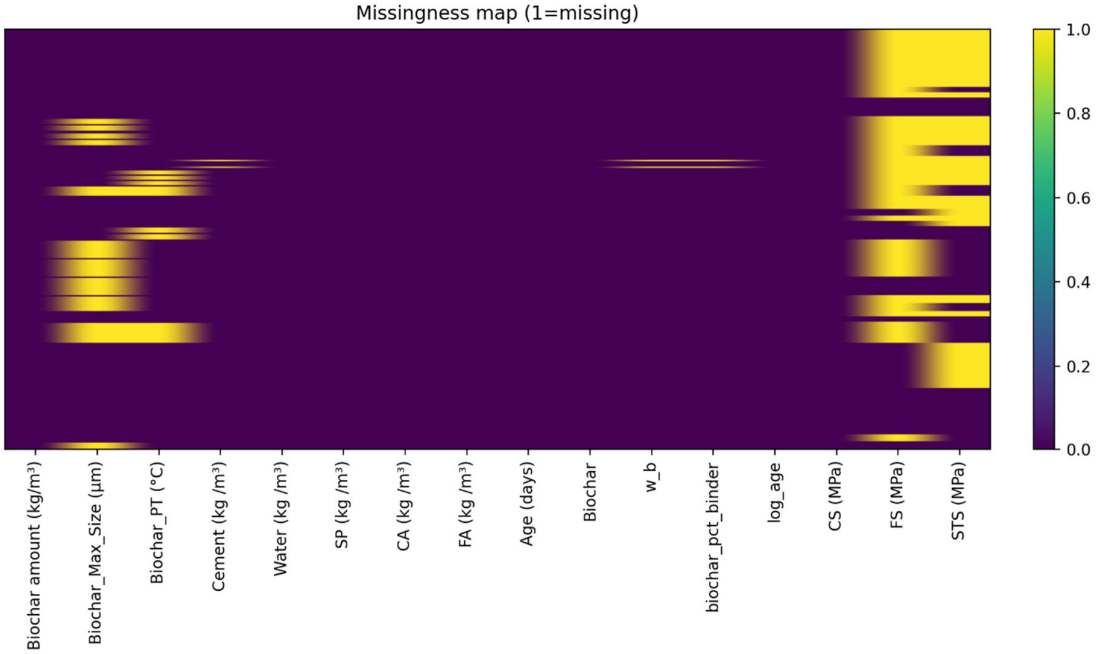

Figure 4. Missingness map.

A correlation heatmap was generated to visualize the Pearson correlation coefficients between all input features and target variables, as shown in Figure 5. This analysis helped identify linear relationships and potential multicollinearity among features, providing preliminary insights into the factors influencing concrete strength [63].

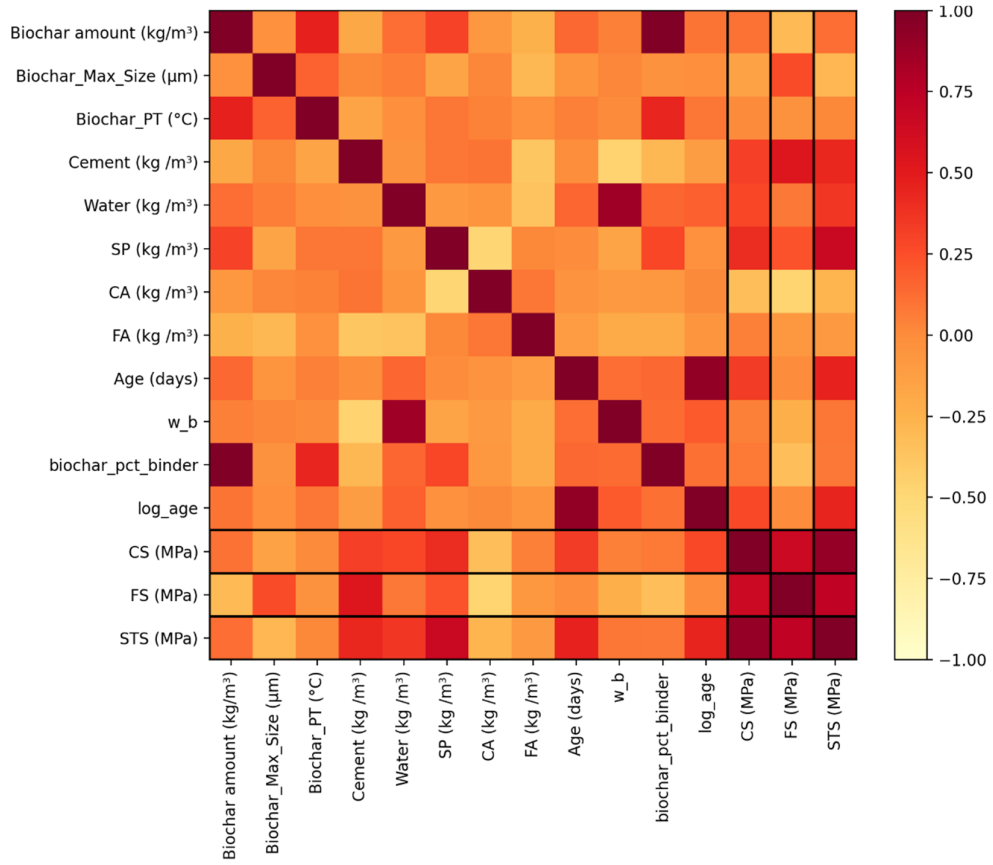

Figure 5. Correlation heatmap of input features and target variables.

2.2.2. ML Setup

The framework of modeling was created as a multi-output regression problem, predicting up to three mechanical properties simultaneously, including CS, STS and FS of the concrete. Multi-target learning was implemented using MultiOutputRegressor, which wraps a single base regressor to independently model each output while maintaining a unified training pipeline [64]. The dataset was partitioned randomly into training and testing sets using a split ratio (80:20), resulting in 254 samples for training and 64 samples for testing. To ensure reproducibility, the split was performed with a fixed random seed of 42.

A regularized linear baseline model was implemented using Ridge regression (Ridge, α = 3.0) as a reference in a multi-output configuration. The model performance was estimated using 5-fold cross-validation. Two tree-based ensemble regressors, RF and GBR, were evaluated. Hyperparameters were optimized using RandomizedSearchCV with 5-fold cross-validation in the inner loop. Model generalization performance was assessed using nested cross-validation (5 outer folds), reporting the mean and standard deviation of RMSE, MAE, and R^2 [65]. The RF model was selected based on nested cross-validation results as the final predictive model. The optimal configuration of the model is given in Table 5.

The final multi-output RF model was serialized using joblib (1.1.0) to ensure reproducibility and facilitate deployment, and was refitted on the complete dataset subset with non-missing target values.

Table 5. Optimal configuration of the RF model.

Parameter	Value	Description
*n*_estimators	1000	Number of decision trees in the RF model. Increased model stability and reduced variance.
max_depth	None	Maximum depth of each decision tree. Unlimited depth allows full tree expansion and captures more complex nonlinear patterns.
max_features	1	Proportion of input features randomly considered at each split (50% of features). This increases tree diversity and reduces correlation between trees.
min_samples_split	2	Minimum number of samples required to split an internal node. This has allowed detailed splitting.
min_samples_leaf	1	Minimum number of samples required at a leaf node. Detailed modeling of local patterns due to a smaller value.

2.2.3. Model Evaluation

The ML models were evaluated based on three standard regression metrics: The Coefficient of Determination (R^2) measures the proportion of variance in the target variable set in the model, ranging from 0 to 1; values close to 1 indicate better model output. Root Mean Square Error (RMSE) measures the average magnitude of prediction errors, with lower values indicating better accuracy. Mean Absolute Error (MAE) measures the average absolute difference between predicted and actual values, providing a more interpretable measure of prediction accuracy. A model performs better with a higher R^2 value and lower MAE and RMSE values; their mathematical expressions are given in Equations (1)–(3), respectively [66].

$$R^2 = 1 - \frac{\sum_{i=1}^{n}(y_i - \hat{y}_i)^2}{\sum_{i=1}^{n}(y_i - \overline{y})^2} \quad (1)$$

$$RMSE = \sqrt{\frac{1}{n}\sum_{i=1}^{n}(y_i - \hat{y}_i)^2} \quad (2)$$

$$MAE = \frac{1}{n}\sum_{i=1}^{n} |y_i - \hat{y}_i| \quad (3)$$

Whereas n is the number of data points, y_i represents actual values, $\bar{y}$ represents the mean of the actual values, and $\hat{y}_i$ represents the projected value.

2.2.4. Model Interpretation and Uncertainty Quantification

Interpretation of the model predictions and feature contributions was achieved using SHAP analysis. In SHAP analysis, each feature is assigned a contribution value for each prediction, which enables both local and global interpretation of model performance. Similarly, Partial dependence plots envision the subsidiary effect of individual features on predicted strengths while averaging over the effects of all other features. Additionally, the CS being the prominent strength characteristics and due to the greater dataset, was selected for Pareto analysis to identify the optimum mix design to achieve maximum CS at minimal cement content. To investigate the effect of various biochar feedstocks on the CS, FS and STS, superimposed effect curves were generated for all biochar types. For each type, predictions were made across a range of biochar dosages while keeping all other features at their median values. To quantify predictive uncertainty, separate quantile Gradient Boosting models were trained for each target using the quantile loss function at α = 0.05, 0.50, and 0.95. These models produced lower (5th percentile), median (50th percentile), and upper (95th percentile) estimates, forming 90% prediction intervals. The quantile models were saved and applied at prediction time to generate uncertainty bounds alongside point predictions. Calibration plots were used to compare nominal and empirical coverage.

All the modeling was implemented in Python (3.9.13) using scikit-learn (1.0.2) for preprocessing, model development, hyperparameter tuning, and validation; SHAP (0.41.0) for

explainability; NumPy (1.21.5) and Pandas (1.4.3) for data handling; and Matplotlib (3.5.2) for figure generation. Trained models were serialized using joblib to ensure reproducibility and facilitate deployment.

3. Results and Discussions

3.1. Experimental Results

3.1.1. Fresh Concrete Properties

The fresh properties of the biochar-enhanced concrete were evaluated by slump, fresh density, and air content. The fresh concrete test results are given in Table 6. The workability and air content test results are given in Figure 6.

Table 6. Fresh concrete test results.

Mix Type	Slump Value (mm)	Fresh Density (kg/m^3)	Air Content (%)
BC0	86.00	2301.49	4.10
BC2	82.00	2304.67	3.97
BC4	76.00	2312.10	3.66
BC6	71.00	2290.87	4.55

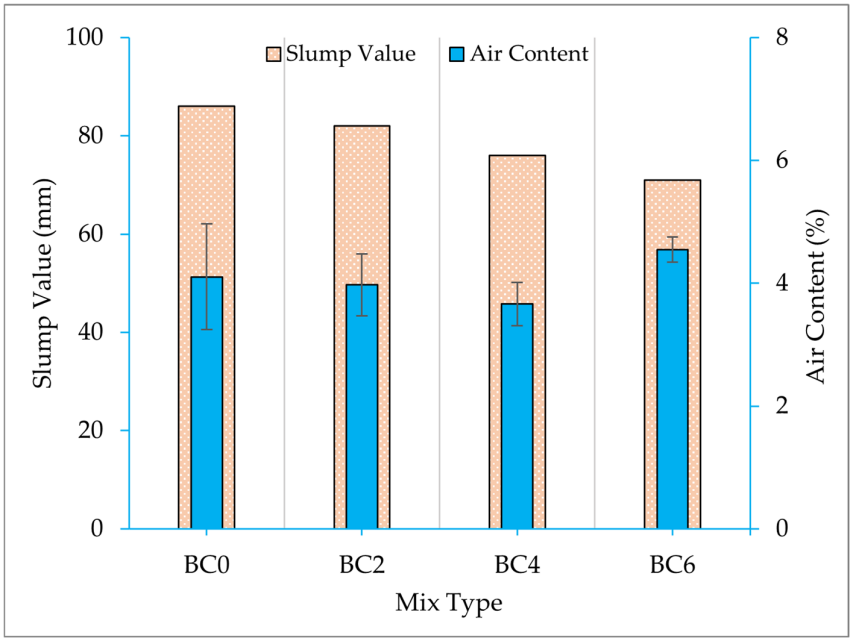

Figure 6. Slump and air content test results.

The high specific surface area and porous morphology of biochar make it hydrophilic during the initial mixing stages of the concrete if used in a dry state, due to which it reduces the workability of the concrete mix [12]. The experimental results show a reduction in the workability of the biochar-modified mixes as compared to the control mix. BC2 mix has experienced 4.65%, BC4 has 11.63%, whereas BC6 exhibits 17.44% reduction in workability. A study reported a decrease of around 13% decrease in workability with the addition of 5% biochar with a maximum particle size of 200 µm [67]. Similarly, the addition of biochar at a higher percentage can significantly reduce the flow characteristics, which can be seen in BC6 concrete mix. Similarly, the particle size or surface area has also shown an impact on the flow characteristics of the concrete mix. A reported value of 10% slump reduction [68] with biochar particle size of 500 µm, as compared to the 17.44% with a 75 µm size biochar of this study, explains that the reduction in biochar particle size bears a high surface area and reduces the workability. The overall reduction in the workability of concrete with

biochar is attributed to the porous structure of the biochar and its water capture ability and dilution effect at higher replacements.

Density of concrete is an important attribute of its strength and durability. The density of biochar affects the density of cement composites. The use of high-carbon-content biochar is suitable for concrete production as a partial replacement of cement; however, it has a lower density [69]. The fresh density altered marginally with increasing biochar content, consistent with the lower specific gravity of biochar compared to cement [70]. The control mix has a density of 2301.49 kg/m^3, the BC2 mix has a density of 2304.67 kg/m^3, BC4 has 2312.10 kg/m^3, and the BC6 has 2290.87 kg/m^3. The fresh state density of biochar modified cement composites ranges from 2245 to 2330 kg/m^3 [71]. It can be noted that up to 4% biochar incorporation, the density is slightly increased, and at 6% incorporation, a slight decrease has been observed as compared to the control mix; however, the variation is not significant. Biochar exhibits low density and high porosity, which affects the overall density when used at higher percentages; however, at lower percentages, the density is almost equivalent to the control mix [68], because it occupies the pores in the matrix and improves the packing density of the concrete mix. The percentage variations are given in Figure 7.

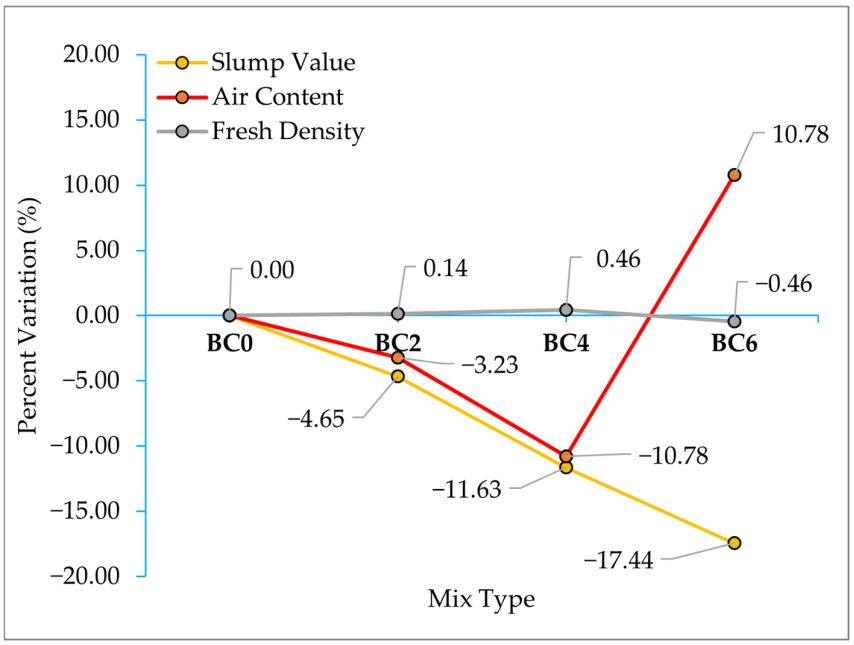

Figure 7. Percent variation in slump value, air content and fresh density of concrete w.r.t the control mix.

Air content for mix types BC0, BC2, BC4, and BC6 are 4.10%, 3.97%, 3.66%, and 4.55%, respectively, indicating that BC4 yields the lowest measured air content among the tested mixtures. Biochar incorporated concrete mixes show a reduction in air content by 3.23% and 10.78% in the BC2 and BC4 mixes, whereas a 10.78% increase was observed in the air content of BC6 as compared to the BC0 mix type. This suggests a threshold beyond which the porous structure of biochar can reintroduce additional entrapped air or reduce workability, facilitating air void formation [15]. These findings align with the concept of the biochar capacity of filling internal pores at lower to moderate levels and improving the packing density of the concrete mix.

3.1.2. CS Performance

The CS of plain and biochar-enhanced concrete mixes BC2, BC4 and BC6 are presented in Figure 8 at 7 and 28 days of testing. The results show improvement in the CS values for all the mixes, both at 7 and 28 days. All the biochar incorporated mixes showed higher

strengths as compared to the control mix; however, the maximum increase was observed at 2% incorporation. BC2 strength values are 50.38 MPa and 63.28 MPa at 7 and 28 days, corresponding to an increase of 7.33% and 9.67%, respectively. Similarly, the strength gain at 28 days is more than the strength gain at 7 days for all samples. Similar trends have been reported on the CS up to 5% incorporation of biochar [72]. The improvement could be attributed to improved packing density of the concrete mixes with biochar filling the pores. Additionally, the biochar pores act as micro water tanks, which promote enhanced continued hydration due to internal curing [12]. The CS percent variation in biochar incorporated concrete as compared to the control mix is given in Figure 9. The strength showed an increase in BC2, BC4 and BC6 of 7.33%, 3.96% and 0.48% at 7 days and 9.67%, 4.37% and 1.12% at 28 days, respectively, as compared to the control mix. This enhancement could be attributed to the filler effect, internal curing and improved hydration of the concrete matrix.

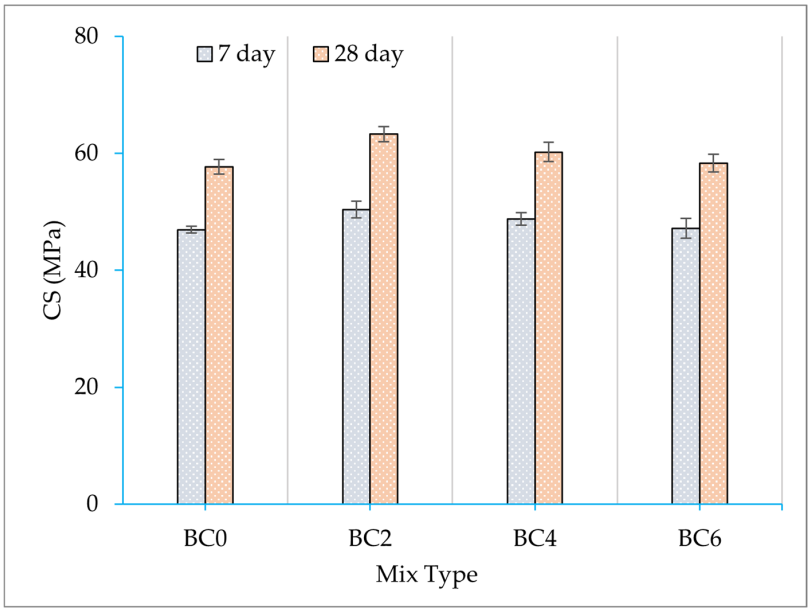

Figure 8. CS of concrete mixes at 7 and 28 days.

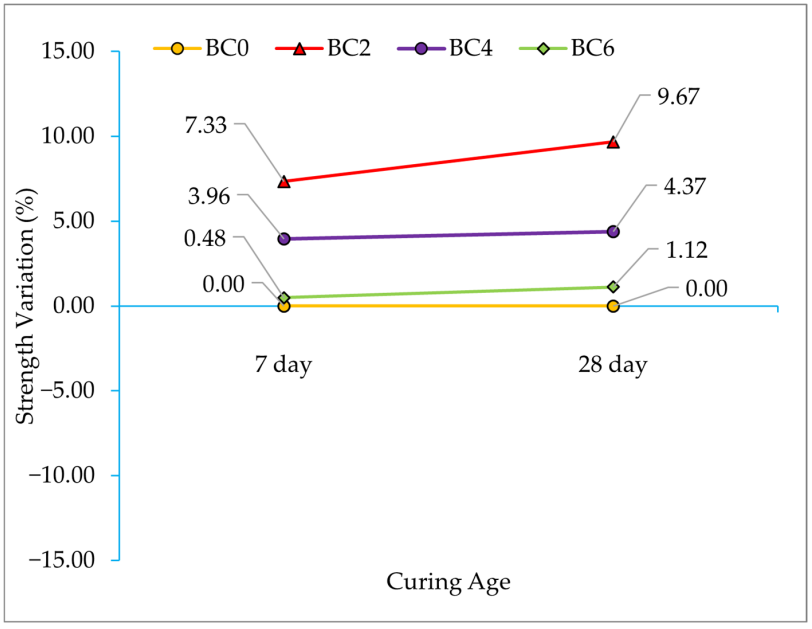

Figure 9. CS percent variation w.r.t. the control mix at 7 and 28 days.

3.1.3. STS Performance

The STS of control and biochar-enhanced concrete mixes BC2, BC4 and BC6 are presented in Figure 10 at 7 and 28 days of testing. The STS percent variation in biochar incorporated concrete as compared to the control mix is given in Figure 11. The results depict improvement in the STS values for BC2 and BC4, both at 7 and 28 days, whereas BC6 has experienced a reduction in strength as compared to the control mix. The maximum increase was observed at 2% incorporation of the biochar in the concrete. The BC2 strength values are 3.07 MPa and 3.98 MPa at 7 and 28 days, corresponding to an increase of 5.69% and 6.24%, respectively. The BC4 strength values are 3.06 MPa and 3.85 MPa at 7 and 28 days, corresponding to an increase of 5.10% and 2.89%, respectively. The strength at 6% replacement has shown a decrease of 3.92% and 1.37%, corresponding to the strength values of 2.79 MPa and 3.69 MPa at 7 and 28 days, respectively. This enhancement could be attributed to the filler effect, internal curing and improved hydration of the concrete matrix. A study reports that the cement-based composites containing biochar 0.1 to 5% have an STS range from 1.9 to 4.9 MPa [71]. The optimum biochar content for the STS is 2%; however, the utilization of 4% is feasible, as the strength is more than the control mix at 4% incorporation. The effect of biochar inclusion is more prominent in the improvement of CS as compared to STS. The influence on the STS is effective when biochar is used as filler instead of cement replacement [71]. The reduction in strength at 6% incorporation of biochar could be attributed to the dilution effect and the porous structure of the matrix, which results in the weaker matrix and crack-bridging capabilities.

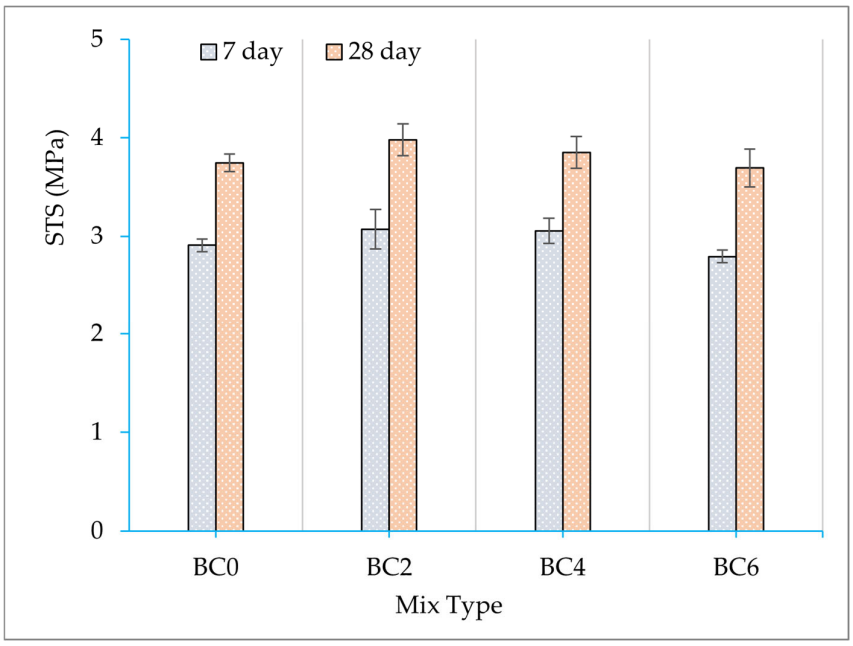

Figure 10. STS of concrete mixes at 7 and 28 days.

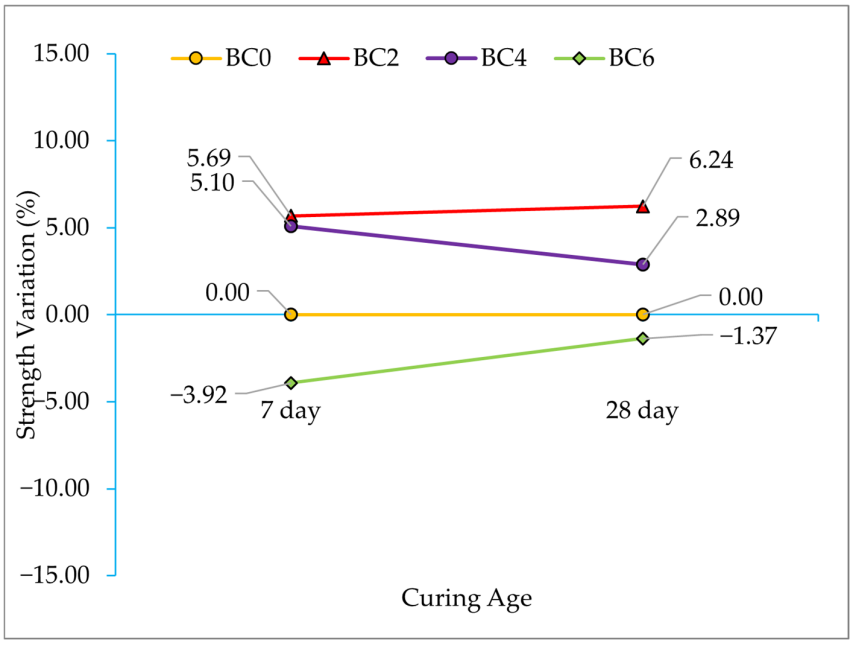

Figure 11. STS percent variation w.r.t control mix at 7 and 28 days.

3.1.4. FS Performance

The FS of control and biochar-enhanced concrete mixes BC2, BC4 and BC6 are presented in Figure 12 for 28 days of testing. All the biochar incorporated mixes showed higher strengths as compared to the control mix; however, the maximum increase was observed at 4% incorporation. The BC4 strength values are 6.52 MPa, corresponding to an increase of 15.4%. Similar trends have been reported on the CS up to 5% incorporation of biochar [72]. The improvement could be attributed to improved packing density of the concrete mixes with biochar filling the pores and improved hydration. The FS percent variation in biochar incorporated concrete as compared to the control mix is given in Figure 13. The strength showed an increase in BC2, BC4 and BC6 of 7.54%, 15.40% and 6.99 at 28 days, respectively, as compared to the control mix. This enhancement could be attributed to the filler effect, internal curing and improved hydration of the concrete matrix.

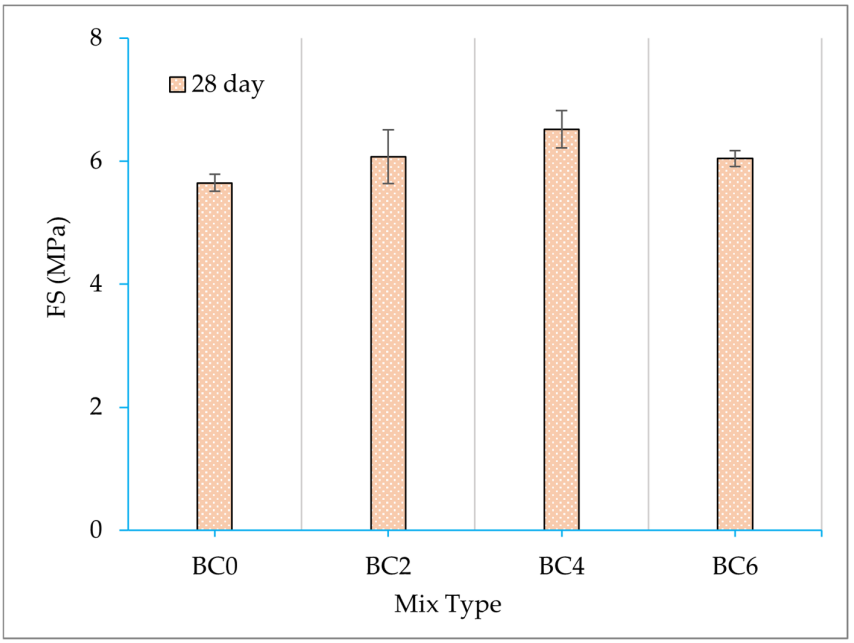

Figure 12. FS of concrete mixes at 28 days.

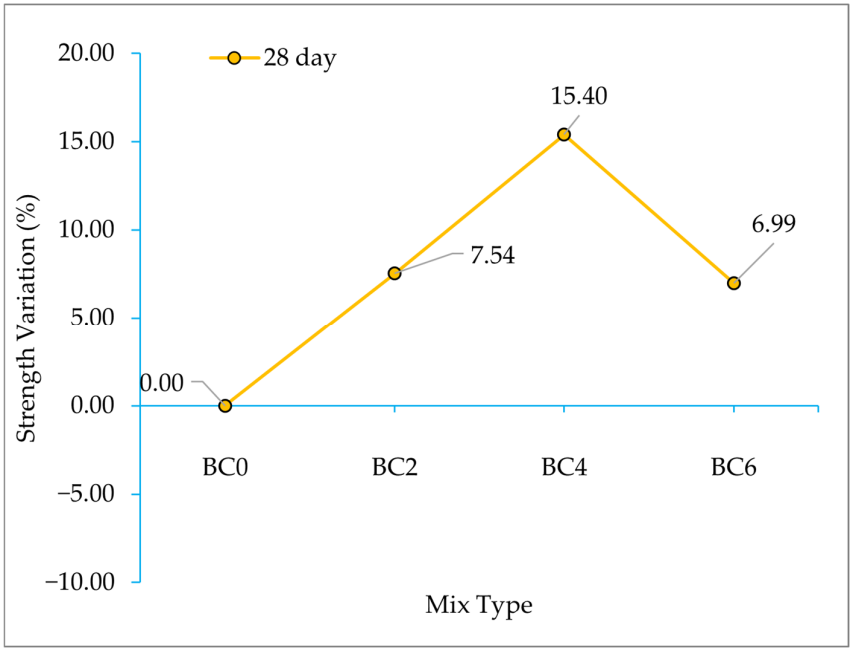

Figure 13. FS percent variation w.r.t control mix at 28 days.

3.2. ML Results

Model Indices and Target Specific Performance

The RF model was examined against the Ridge regression baseline model using nested-cross-validation. Performance indices of both models are given in Table 7. The optimized RF model with nested cross-validation exhibits higher predictive performance than the Ridge regression baseline model. The RF exhibits R^2 of 0.817 ± 0.072, RMSE of 2.08 ± 0.31 MPa, and MAE of 1.12 ± 0.15 MPa, which corresponds to an improvement of 9.08% in R^2 and a reduction of 32.47% in RMSE and 32.12% in MAE values compared to the Ridge baseline model. Similarly, the lower values of standard deviation throughout the 5 folds, the R^2 of 0.072, RMSE 0.31 MPa and MAE 0.15 indicate a stable performance of models through various data partitions with good generalization attributes. Similar trends have been reported by previous studies using ensemble methods outperforming the linear models for the prediction of concrete properties [23,24,72].

Table 7. Performance indices of ML models.

Model	Validation Method	R^2	RMSE (MPa)	MAE (MPa)
RF	Nested CV (5 × 5)	0.817 ± 0.072	2.08 ± 0.31	1.12 ± 0.15
Ridge Regression	5-fold CV	0.749	3.08	1.65

The RF model was tested on the held-out test, 20% of the data set, to evaluate the model's ability to predict individual target parameters of CS, FS and STS of biochar-modified concrete mixes. Figure 14 shows the actual versus predicted plots for each target variable (a) CS, (b) STS, and (c) FS, with R^2 values displayed in the legend both for training and testing of the model. Table 8 summarizes the testing R^2 values for each target variable.

Table 8. Target the specific performance of the RF model.

Target	Sample Size (n)	Training R^2	Testing R^2
CS	318	0.985	0.894
FS	126	0.991	0.828
STS	159	0.959	0.537

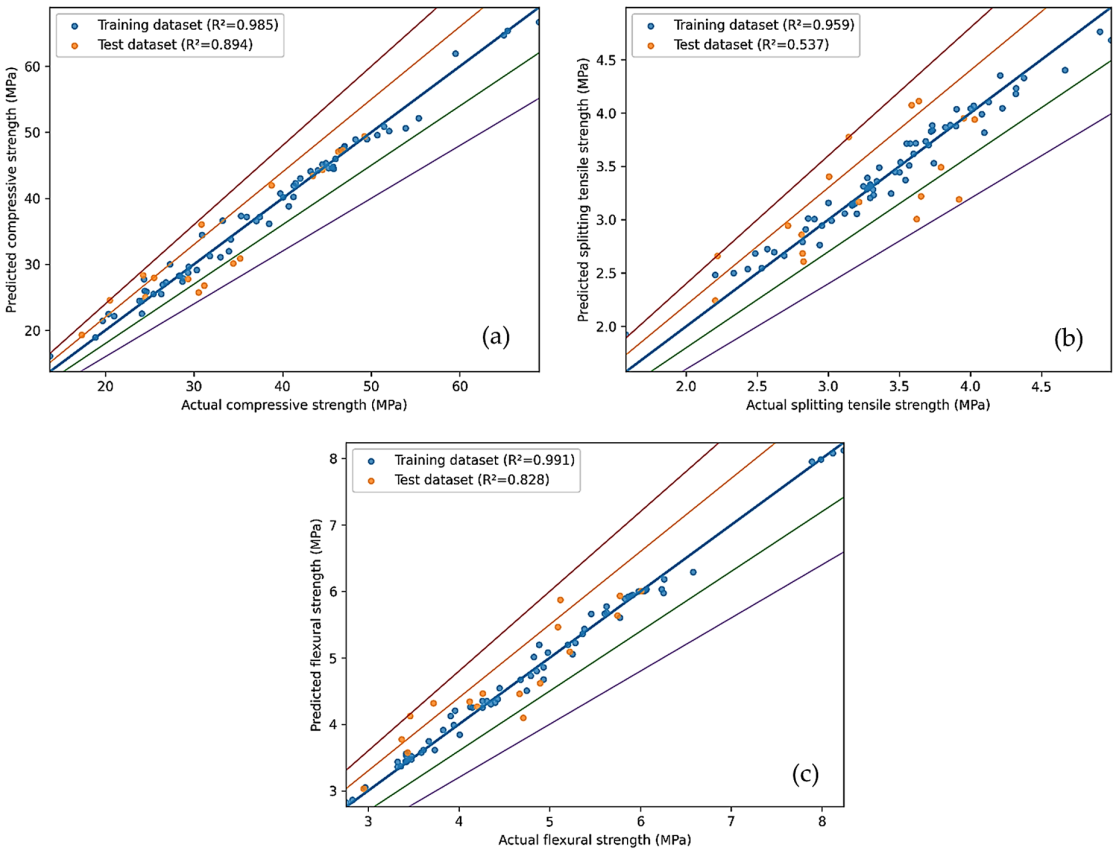

Figure 14. Prediction plots of the RF model after optimization: (**a**) CS; (**b**) STS; (**c**) FS.

The RF model demonstrated the prediction of CS of the biochar-enhanced concrete with accuracy, with a testing R^2 of 0.894. The RF model performance can be linked to a sufficient dataset (n = 318) and a strong physical relation between the input parameters and CS [73]. The small gap between training (0.985) and testing (0.894) of R^2 values indicates good generalization without substantial overfitting. Similarly, for FS, the RF model achieved an R^2 value of 0.828, indicating a good performance level despite having only 126 samples. This is particularly noteworthy as FS is often more variable than CS due to its sensitivity to microcracks, aggregate distribution, and interfacial transition zone properties [74]. At the same time, the model showed moderate performance for STS with an R^2 value of 0.537, with a train-test gap of 0.422. This could be attributed to the complex nature of biochar effects on tensile strength properties of concrete mixes. Similarly, STS is more sensitive to specimen preparation, loading alignment, crack initiation, interfacial transition zone behavior, and microstructural variability [75]. Also, the limited sample size (n = 159) may not fully reflect the concrete mix design diversity. The residual plot also shows wider scatter for STS, confirming higher uncertainty. However, the overall nested cross-validation result, R^2 = 0.816, suggests that the model is not unstable. The lower STS performance is therefore attributed mainly to physical variability and insufficient feature representation of tensile failure mechanisms. The inherent variability of STS testing could be a cause that is sensitive to loading conditions and preparation of specimens. The STS predictions should be interpreted with greater caution than CS and FS.

3.3. Experimental vs. Predicted Results

The model is designed to provide two types of strength predictions. The RF point estimates are from the optimized RF model, which serves as the single-value prediction for each strength property of the concrete. The prediction intervals q05, q50 and q95 are

from quantile Gradient Boosting models, which quantify the associated uncertainty of the predicted values. The prediction intervals indicate the range within which the true value is expected to fall with 90% confidence. The experimental and predicted strength values for the primary RF model and quantile prediction intervals are given in Table 9. This dual-output approach enhances the practical utility of the model by enabling users to assess both the most likely strength and the reliability of each prediction.

Table 9. Experimental and predicted values of concrete mixes at 7 and 28 days.

Property	Mix Type	Experimental and Predicted 7-Day Strength Values (MPa)					Experimental and Predicted 28-Day Strength Values (MPa)				
		Exp	RF Point	q05	q50	q95	Exp	RF Point	q05	q50	q95
CS	BC0	46.94	35.85	29.64	41.96	57.97	57.70	45.78	36.13	48.96	63.76
	BC2	50.38	36.33	31.35	46.88	57.65	63.28	47.79	37.63	53.07	64.25
	BC4	48.80	35.26	31.42	45.74	58.83	60.22	46.76	37.70	51.91	65.40
	BC6	47.16	34.48	31.45	44.79	59.17	58.34	44.70	37.74	50.91	65.65
STS	BC0	2.91	3.76	2.96	3.51	3.96	3.74	4.04	3.39	4.07	4.56
	BC2	3.07	3.74	2.94	3.45	3.98	3.98	4.03	3.41	4.04	4.59
	BC4	3.06	3.58	2.94	3.18	3.99	3.85	3.91	3.41	3.96	4.59
	BC6	2.79	3.47	2.72	2.97	4.00	3.69	3.71	3.18	3.73	4.60
FS	BC0	-	5.25	4.78	4.48	5.18	5.65	5.76	4.79	5.29	6.77
	BC2	-	5.24	4.90	4.61	5.20	6.07	5.78	4.91	5.38	6.79
	BC4	-	5.32	4.91	4.69	5.20	6.52	5.79	4.91	5.43	6.80
	BC6	-	5.28	4.92	4.77	4.91	6.04	5.67	4.92	5.56	6.37

3.3.1. CS Prediction

The result of CS shows that 2% biochar replacement gives optimum results both at 7 and 28 days of testing. The prediction of q50 best suits the CS of the biochar concrete, which is preferable for application rather than overestimation. Figure 15 presents the experiment versus the predicted 7-day CS and corresponding strength variations. At 7 days, the RF model predictions underestimated the values across all mixes, which could be attributed to the dataset, as most of the data pertained to 28-day strength. Also, this research is based on high-strength concrete, so the data pertaining lies above the predicted values and potentially underrepresents the rapid early-age strength development using biochar and cement type. The median predictions (q50) showed closer agreement with experimental values for the 7 days, with strength variation from −10.59 (BC0) to 5.03% (BC6), suggesting that the quantile model provides more accurate central tendency estimates at an early age.

Figure 16 presents the experimental versus predicted 28-day CS and corresponding strength variations. At the age of 28 days, the RF model predictions improved with strength variation between −20.66% (BC0) and −24.48% (BC2) as compared to the 7-day prediction. Similar to 7-day strength predictions, the 28-day prediction is in better agreement with median predictions q50. The strength variation for q50 is −15.14% for BC0, −16.13% for BC2, −13.79% for BC4, and −12.73% for BC6. Notably, all experimental values fell within the 90% prediction intervals between q05 and q95, which ranged from 36.13 to 63.76 MPa for BC0 to 37.74–65.65 MPa for BC6, indicating that the model's uncertainty quantification effectively captures the true values.

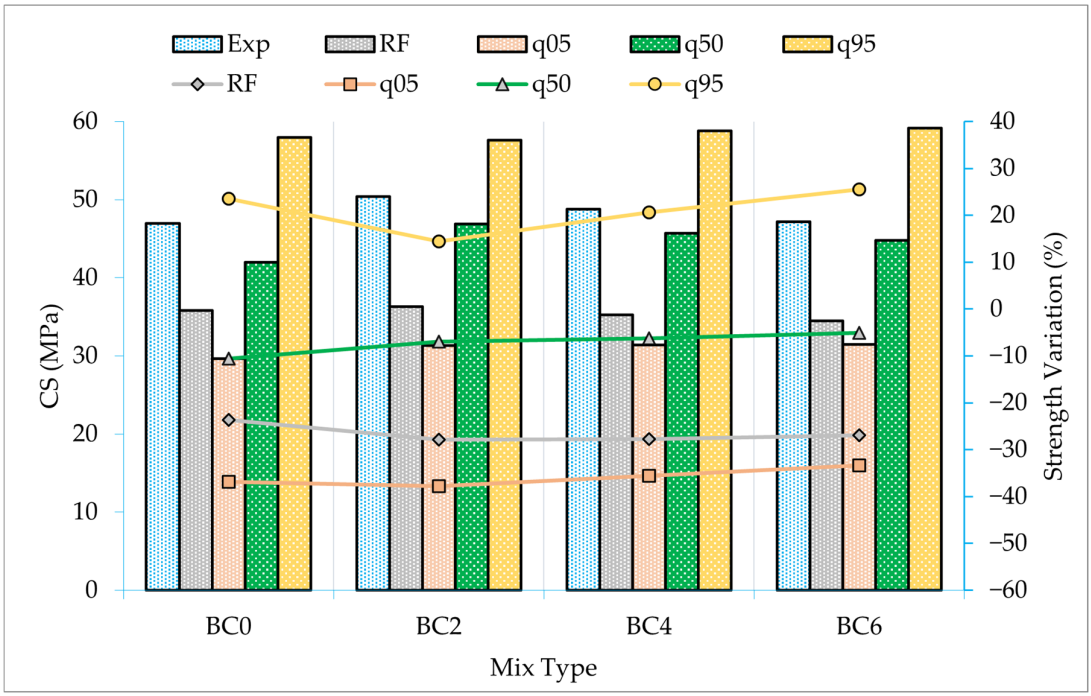

Figure 15. Experimental vs. predicted 7-day CS and corresponding strength variations.

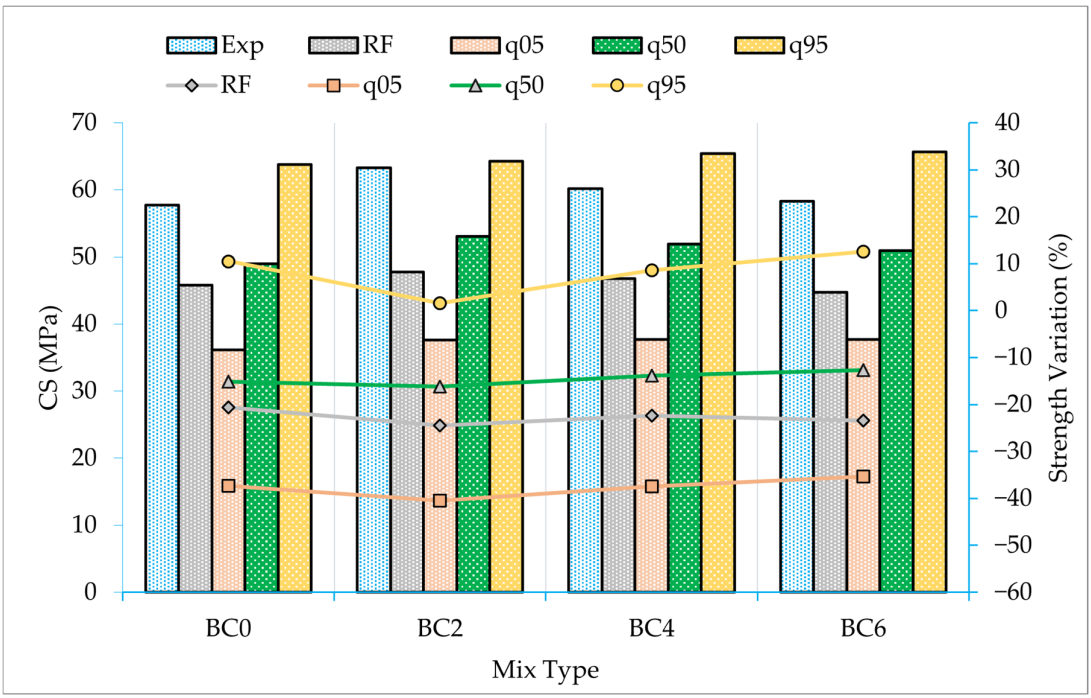

Figure 16. Experimental vs. predicted 28-day CS and corresponding strength variations.

3.3.2. FS Prediction

At 28 days, the experimental FS is more consistent with the RF model point predictions across all mixes, with strength variation ranging from −4.90% (BC2) to −11.12% (BC4) as compared to experimental results. Figure 17 presents the experimental versus predicted 28-day FS and corresponding strength variations. Similarly, the median prediction q50 showed a similar trend with strength variations of −6.28% for BC0, −11.42% for BC2, −16.69% for BC4, and −7.93% BC6 as compared to experimental results of the relevant mixes. The BC4 showed the optimal results experimentally achieving 6.52 MPa, repre-

senting a 15.4% increase over the control mix (5.65 MPa). The model predicts the same trend both with the RF model point and median predictions at BC4 with 5.79 MPa and 5.43 MPa, respectively. The predictions are slightly underpredicted as the model may not fully capture the crack-bridging mechanisms and improved interfacial transition zone properties. However, the 90% prediction intervals ranged from 4.79 to 6.77 MPa for BC0 to 4.92–6.37 MPa for BC6, capturing the experimental values for BC0, BC2, and BC6, but fell slightly below the experimental value for BC4, with a value of 6.52 MPa vs. the upper bound 6.80 MPa, indicating that the model's uncertainty range marginally underestimated the optimal FS at 4% replacement. This highlights the prospect of biochar for flexural applications, such as using it in pavements and slabs. However, the model exhibited the largest prediction variations for FS, particularly at the optimal 4% dosage. It suggests that the complex mechanisms governing flexural behavior, including aggregate interlocking and crack bridging effects, need to be studied and incorporated. The in-depth understanding of FS across all mixes in data indicates that additional data, particularly for mixes with higher biochar dosages, would further improve model performance for this critical property.

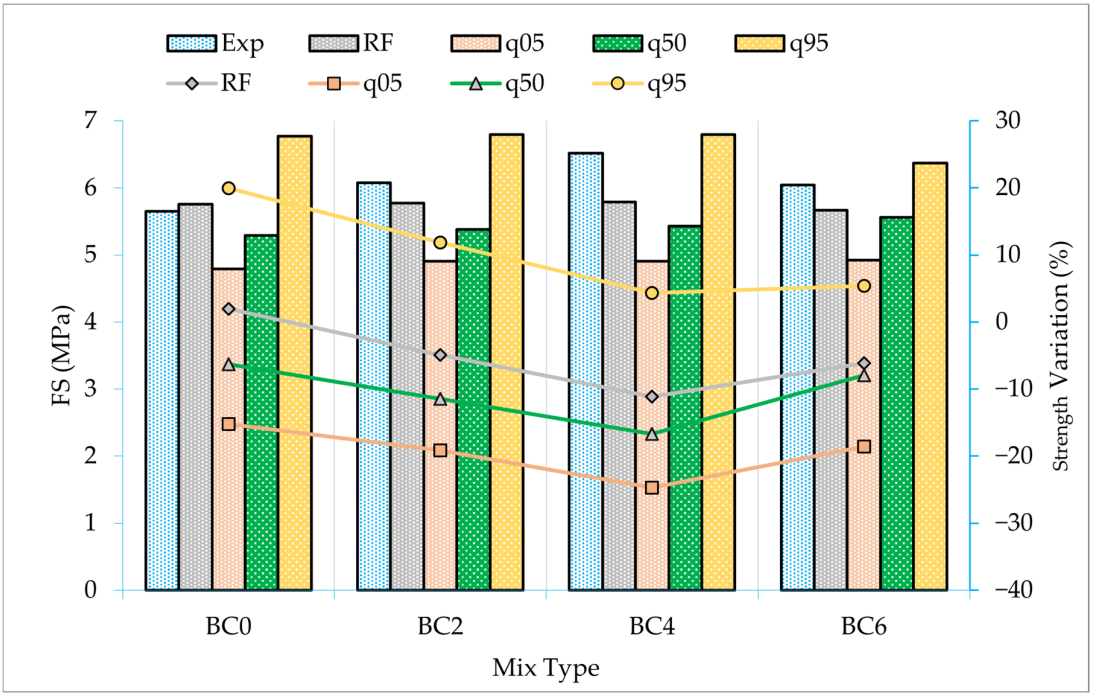

Figure 17. Experimental vs. predicted 28-day FS and corresponding strength variations.

3.3.3. STS Prediction

At 7 days, the RF model predictions overestimate the values across the mixes in contrast to CS. Figure 18 presents the experimental versus predicted 7-day STS values and their corresponding strength variations. The experimental STS values at 7 days for BC0, BC2, BC4 and BC6 were 2.91 MPa, 3.07 MPa, 3.06 MPa, and 2.79 MPa, respectively. The RF model predictions for these mixes observed were from 3.76 MPa for BC0 to 3.47 MPa for BC6, corresponding to strength variations of 29.48% and +17.33%. The q50 median predictions showed enhanced agreement, with strength variations of +20.85% for BC0, +12.43% for BC2, +4.16% for BC4, and +6.51% for BC6. Notably, for BC6 and BC4, the median predictions were within 5% of experimental values, indicating that the quantile model captures the optimal dosage trend more accurately. All experimental values fell within the 90% prediction intervals, which ranged from 2.96 to 3.96 MPa for BC0 to 2.72–4.00 MPa for BC6, confirming adequate uncertainty coverage.

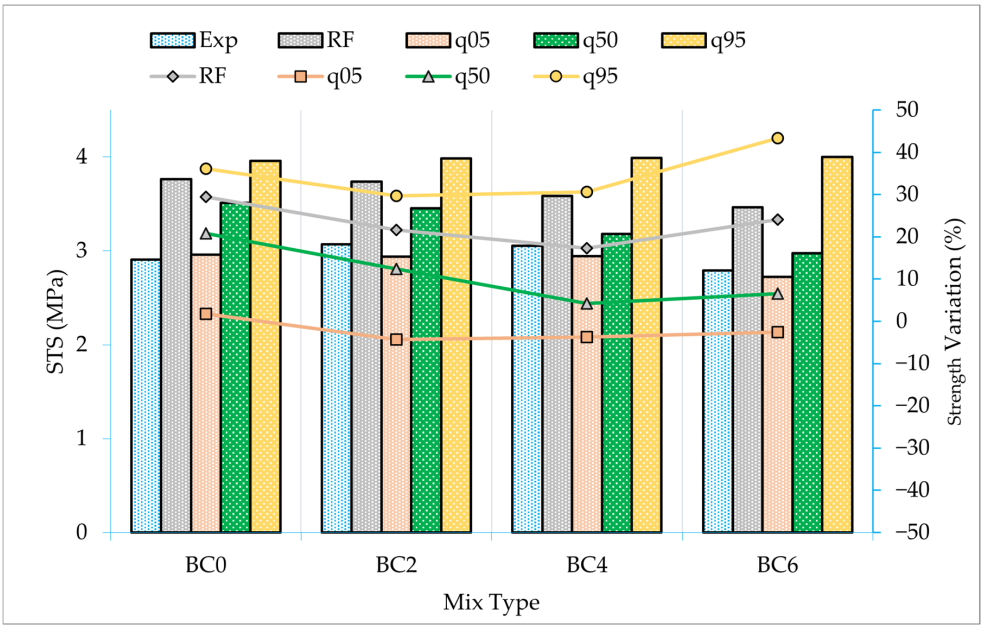

Figure 18. Experimental vs. predicted 7-day STS and corresponding strength variations.

Figure 19 presents the experimental versus predicted 28-day STS values and their corresponding strength variations. The RF model point predictions are more prominent at 28 days, with strength variations ranging from +0.48% for BC6 to +7.89% for BC0. The q50 median predictions also showed good compliance with experimental results; the corresponding strength variation for BC0, BC2, BC4, and BC6 are +8.61%, +1.63%, +2.70%, and +0.93% respectively. The closest prediction for BC6 with a strength variation of only +0.48% highlights the model's ability to predict the later age STS accurately. BC2 was recorded as an optimum mix by gaining a strength of 3.98 MPa with an increase of 6.4% over the control mix, which the model predicted with the same pattern both in the RF model point and meridian. Notably, all experimental values fall within the 90% prediction intervals.

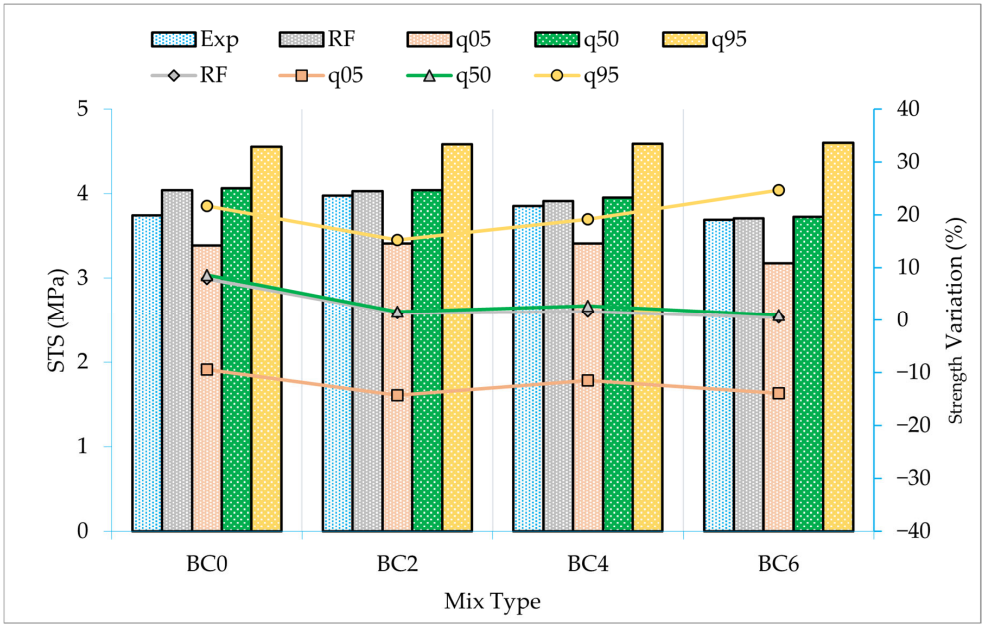

Figure 19. Experimental vs. predicted 28-day STS and corresponding strength variations.

The STS was overpredicted at 7 days but showed close agreement at 28 days. This indicates that the model depicts the later-age tensile properties more accurately than early-age properties, possibly due to the predominance of 28-day data in the training set and the complex behavior of biochar addition to concrete mixing.

3.4. Feature Importance and Directional Effects Using SHAP

SHAP analysis is used to interpret each input feature contribution. Figure 20 depicts the mean SHAP plots presenting global feature importance, (a) CS, (b) FS and (c) STS, in which the features are ranked by their average absolute contribution to model predictions. Figure 21 shows the beeswarm SHAP summary plots representing the magnitude and direction of feature effects. The red points in the plots indicate high feature values, whereas the blue points specify low feature values. The positive SHAP values increase predicted strength.

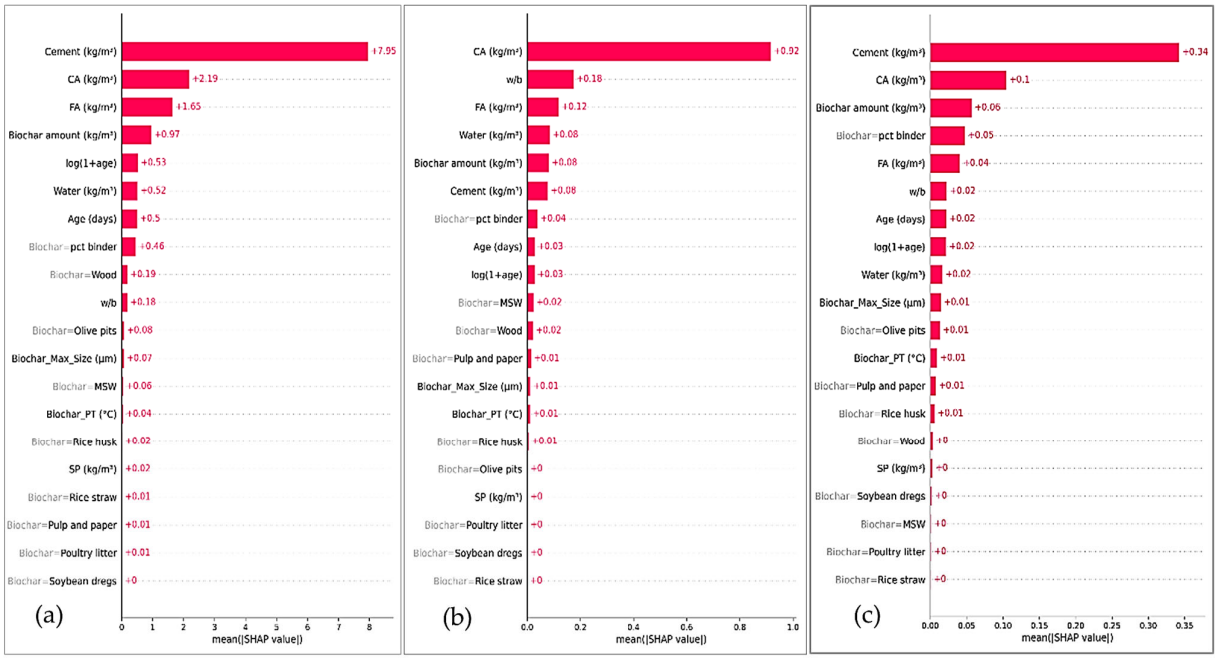

Figure 20. Mean SHAP bar plots of global feature importance: (**a**) CS; (**b**) FS; (**c**) STS.

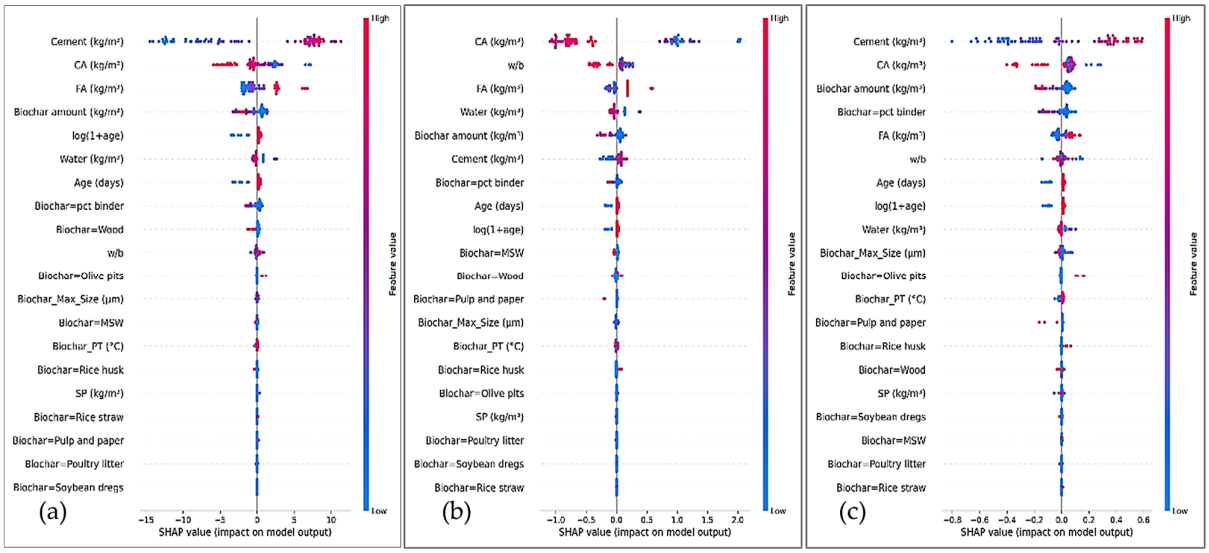

Figure 21. SHAP summary beeswarm plots for: (**a**) CS; (**b**) FS; (**c**) STS.

Cement content emerged as the most effective feature for CS of the concrete mixes, as shown in Figure 20a. This states the most fundamental role in the strength development of concrete. Similarly, CA and FA content also have a high rank, which is in conjunction with their contribution to the matrix density of the concrete [74]. The biochar has a significant effect on the CS and is clearly justified by its presence in the top five features. The SHAP summary plots reveal that higher cement content consistently increases the predicted CS. The water-to-binder ratio exhibits a negative relationship with the concrete matrix. In addition, biochar amount exhibits a complex non-linear behavior with moderate usage from 10 to 30 kg/m^3 increased the predicted strength, whereas high dosage above 50 kg/m^3 showed negative or diminishing effects. Among biochar types, the wood biochar has also shown a notable impact on the prediction values. Additionally, the biochar size, pyrolysis temperature and type have an impact on the CS prediction but can be termed as minimal.

The top five features for the FS from the SHAP analysis are CA, water to binder ratio, FA, water and biochar amount. CA followed by the water-to-binder ratio are the most important features shown by the SHAP analysis and align with the understanding that the FS is highly influenced by the matrix integrity and aggregate interlocking capabilities of the concrete matrix. The SHAP summary plots reveal that they have a positive relationship with the predicted FS values. The water-to-binder ratio exhibits a negative relationship with the prediction values. Among biochar types, the wood biochar after municipal solid waste biochar has also shown a notable impact on the prediction values of FS. Additionally, the biochar size, pyrolysis temperature and type have minimal impact on the FS prediction.

The top five features for the STS from the SHAP analysis are cement content, CA content, biochar amount, biochar to binder ratio and FA content. For STS, cement content followed by CA are the most important features shown by the SHAP analysis. The engineering feature biochar to biochar remains in the top five features for the STS, reflecting the dependence of tensile strength on matrix density and porosity. The water-to-binder ratio exhibits a strong negative relationship with prediction values. Among biochar types, the wood biochar has also had a notable impact on the prediction values. Additionally, the biochar size, pyrolysis temperature and type have an impact on the CS prediction but can be termed as minimal.

3.5. Analysis of Biochar Type on Mechanical Properties

To assess the effect of various biochar types on the mechanical properties of the concrete, superimposed effect graphs were generated from the present dataset for all types of biochar. The biochar dosage for each type was kept at 0 to 120 kg/m^3, and holding all other input parameters at their median values, which enables the direct comparison of biochar type-specific performance. It should be noted that the biochar effect curves show flattened response curves at dosages above approximately 50 to 60 kg/m^3. It is primarily due to the limited data availability at higher dosages of biochar. This leads to flat response surfaces, due to sparse data, and predictions tend to revert to the mean. Additionally, the data set for each type of biochar is not same and similarly the usage of amount of biochar varies significantly, therefore the top three biochar sources are rice husk (n = 69, amount up to 100 kg/m^3), wood (n = 52, amount up to 37 kg/m^3) and bamboo (n = 38, amount up to 43 kg/m^3) biochar. Figure 22 presents the biochar type superimposed effect curves: (a) CS; (b) FS; (c) STS. Other biochar types have limited data, due to which the superimposed curves may overestimate or underestimate the overall behavior.

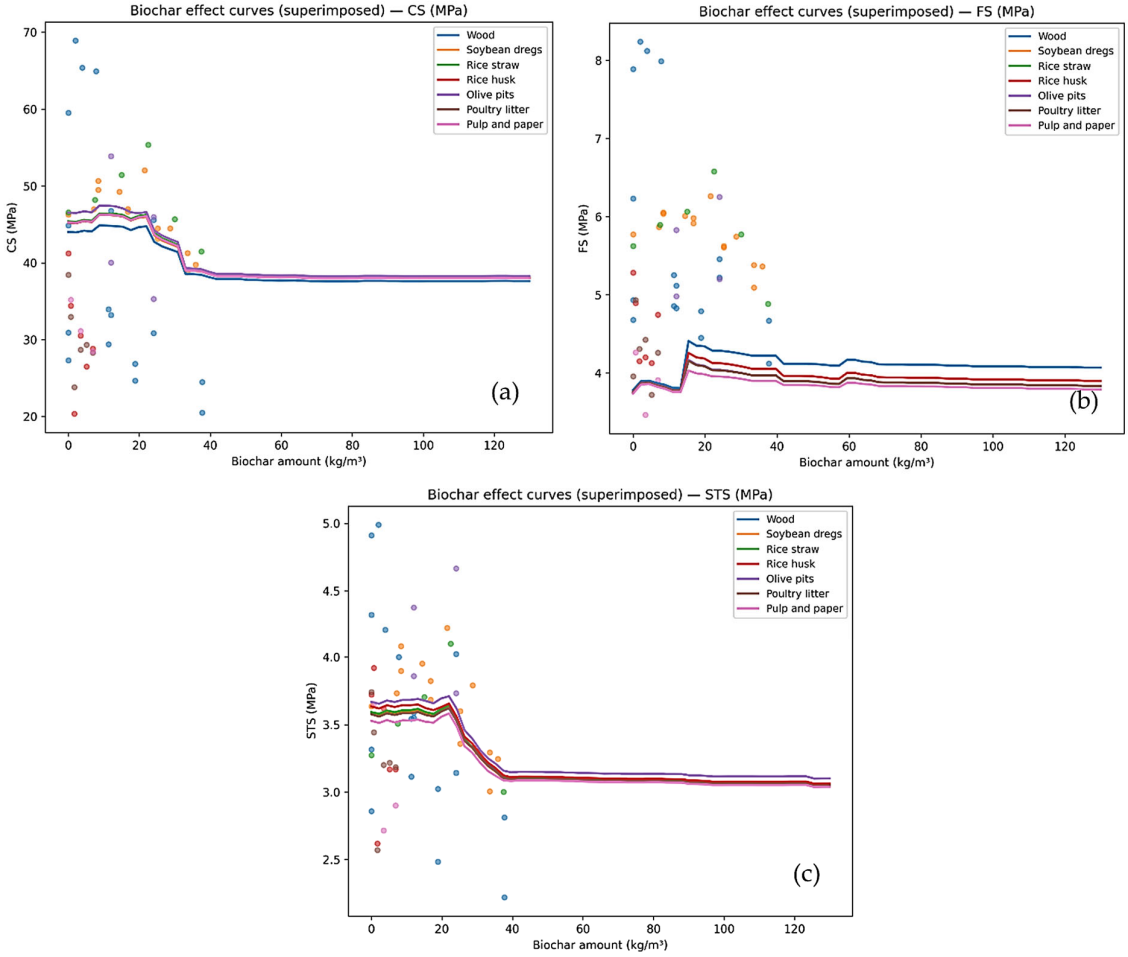

Figure 22. Biochar type superimposed effect curves on the mechanical properties of concrete: (**a**) CS; (**b**) FS; (**c**) STS.

The rice husk biochar and wood waste biochar have a significant influence on the CS prediction and are considered more reliable due to diverse data sets. The rice husk biochar modified concrete exceeds the 55 MPa predicted strength values at optimum dose (at 20–30 kg/m^3), which could be attributed to the high amorphous silica content in this biochar contributing enhanced and secondary hydration product formation due to pozzolanic reactions [47,49]. The wood waste biochar shows up to 50 MPa predicted strength values at optimum dose (20 kg/m^3), followed by a gradual decline at higher replacement, which could be attributed to the saturating effect. Live pits biochar achieves the highest predicted peak strength (62 MPa at 20 to 30 kg/m^3). However, olive pits biochar has only nine samples and soybean dregs have twelve samples in the database. Predictions at higher dosages are therefore extrapolated, and the true behavior of olive pits and soybean dregs biochar beyond the observed range remains uncertain. Soybean dregs biochar limited sample sizes reduce confidence in their ranking curves and optimal dosage predictions for CS performance.

The FS effect curves reveal rice husk biochar as the top performer based on single-point peak values. However, the overall effect curve of the wood biochar remains more prominent, which can be seen in Figure 22b. Rice husk achieves a peak predicted FS of about 6.8 MPa at an optimal dosage of 20 to 40 kg/m^3. This enhanced behavior is due to the largest dataset for rice husk, lending high confidence in the ML findings. The presence of high silica content in the rice husk biochar contributes to pozzolanic reactions, in addition to its favorable particle morphology, making it effective for flexural applications where crack-bridging under loading is considered critical [50]. The second-highest peak (6.2 MPa

at 20 to 40 kg/m^3) predicted for FS was for wood biochar with the flat cure after 40 kg/m^{3,} as higher percentage replacements data is not available. The fibrous structure of wood biochar particles helps effective crack bridging in addition to its low carbon content, which explains its strong FS performance even at moderate replacement levels [51]. Bamboo biochar achieved approximately 6.0 MPa at 20 to 30 kg/m^3, supported by a moderate dataset (n = 38, dosages up to 43 kg/m^3) and could be attributed to the cellular structure of bamboo biochar, influencing FS [54]. Soybean dregs biochar (n = 12) and olive pits biochar (n = 9), limited sample sizes reduce confidence in their precise ranking and optimal dosage predictions for FS performance.

Among the larger data sets of biochar, wood biochar achieved the peak STS of 3.9 MPa at an optimal dosage of 10 to 20 kg/m^3, followed by a sharp decline at higher dosages, and rice husk achieved approximately 3.7 MPa at 10 to 10 to 20 kg/m^3. However, the superimposed effect shows that rice husk is above the wood biochar, which could be attributed to the diversity of the data set among both types. The continuing decline in tensile strength beyond the optimal dosage reflects the competing effects of micro-reinforcement at low dosages versus cement dilution and increased porosity at higher dosages [48]. The decline in STS is sharp compared to CS and FS, which suggests that the dilution effect of cement replacement is more prominent in STS due to the critical nature of the interfacial bond between the aggregate and cement in this case [52].

The optimum biochar dosage varies by type and property of feedstock. The rice husk and wood biochar have the most diverse applications in enhancing the mechanical properties of the concrete. For CS, FS and STS 15 to 30 kg/m^3, 20 to 40 kg/m^3, and 10 to 25 kg/m^3 is recommended, respectively, to optimally utilize biochar in concrete. The wood biochar stands out due to its properties and abundance. It could be a locally available and sustainable option that performs well across all properties. The use of wood biochar should be considered to produce sustainable concrete, as it represents a locally available and sustainable option that performs well across all properties from the UK waste stream.

3.6. Optimization for Sustainable Mix Design

Cement is the most important feature in optimizing the mix design of concrete due to its chemical properties during the hydration process, imparting strength and addressing environmental concerns. Cement has been selected to optimize the mix design with acceptable concrete CS and minimum cement content. Figure 23 presents the Pareto front analysis for CS versus cement amount, classifying optimal mixes that increase strength while reducing cement amount in the mix. The sampled mix design data points are represented by blue points, optimized mix designs are presented by orange, and the green points represent the actual data from the training set. The best trade-offs between concrete performance and environmental impact are presented by the Pareto front analysis optimal solution, which specifies the incorporation of biochar in the range of 15 to 30 kg/m^3. Moderately low mixes with cement less than 350 kg/m^3 can achieve the strength to the tune of 45 MPa with appropriate use of biochar as cement replacements. At lower strength, the Pareto front analysis is steeper, which indicates the diminishing returns with cement addition approximately beyond 400 kg/m^3. This assessment shows how the ML models can provide sustainable insights to sustainable mix design, reducing experimental work and identifying sustainable solutions. The developed mode can be used as a decision support tool for researchers and concrete technologists.

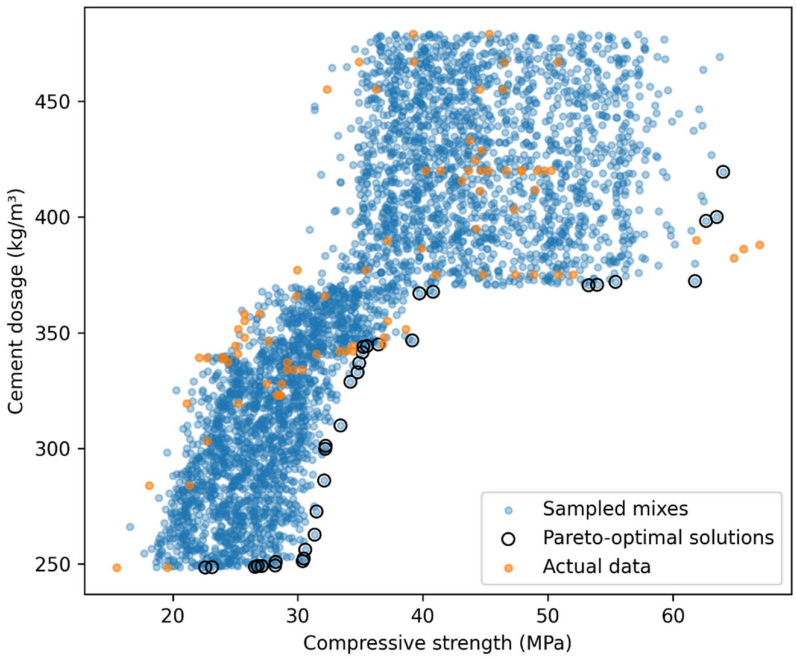

Figure 23. Pareto front analyses the optimal solution for CS versus cement content.

4. Conclusions and Recommendations

This study combined experimental investigation and ML to predict the CS, FS, and STS of wood waste biochar-modified concrete, and feedstock-specific performance characterization. The key findings are summarized below.

4.1. Experimental Findings

The experimental investigation of wood waste biochar at an increment of 0%, 2%, 4%, and 6% as a partial cement replacement by weight in concrete revealed the following findings in fresh concrete properties.

1. The slump decreased progressively from 86 mm (BC0) to 71 mm (BC6), representing reductions of 4.65%, 11.63%, and 17.44% for BC2, BC4, and BC6, respectively. This reduction is attributed to the water absorption capacity and high specific surface area of biochar particles, which absorb mixing water and increase the viscosity of the fresh paste. The use of SP at 0.75% in BCO and 1% in all biochar-added mixture by weight of cement of cementitious material ensured the workability in the relevant slump class.
2. The fresh density of all the concrete mixes showed minimal variation, with BC4 achieving the highest density (2312.10 kg/m^3, +0.46%), while BC6 showed a slight reduction (2290.87 kg/m^3, −0.46%). This marginal decrease at higher biochar content reflects the lower specific gravity of biochar compared to cement.
3. The air content decreased by 3.23% and 10.78% for BC2 and BC4, respectively, indicating improved compaction and particle packing at low to moderate biochar dosages. However, in BC6, air content increased by 10.78%, which could be attributed to the additional air voids shifting the filler effect at lower percentages to saturation at higher percentages.
4. The BC2 mix achieved maximum CS both at 7 and 28 days of testing with corresponding increases of 7.33% and 9.67%, respectively, as compared to the control mix. The BC4 and BC6 achieved 60.22 MPa and 58.34 MPa with an increase of 4.37% and +1.12%, respectively, at 28 days. The increased performance could be attributed to the smaller particle biochar size and internal curing mechanism, extending the hydration period.

5. The optimal STS was achieved by BC2 with 3.07 MPa and 3.98 MPa corresponding to an increase of 5.06% and 6.24% at 7 and 28 days, respectively, as compared to the control mix. A similar trend was recorded for BC4; however, unlike CS, the STS of BC6 experienced a reduction of 3.92% and 1.37% as compared to the control mix. The improvement at 2% and 4% replacement is attributed to the micro-reinforcement of the concrete matrix by the biochar particles, which bridge tensile cracks and improve interfacial bond strength between the cement paste and aggregates. The decline at 6% replacement reflects the detrimental effects of cement dilution, increased porosity, and reduced interfacial bond strength at higher biochar dosages.
6. The FS optimum value was achieved by BC4 mix, reaching 6.52 MPa compared to 5.65 MPa for the control mix, representing a substantial increase of 15.4% at 28 days. The strengths of BC2 and BC6 experienced 7.54% and 6.99% as compared to the control mix. This pronounced enhancement is attributed to a combination of factors, including the fibrous morphology of wood-derived biochar particles that provide effective crack-bridging, the improved interfacial transition zone properties enhance load transfer, and the internal curing effect reduces microcracking.

4.2. ML Findings

1. The optimized RF model achieved a nested cross-validated R^2 of 0.817 $\pm$ 0.072, RMSE of 2.08 $\pm$ 0.31 MPa, and MAE of 1.12 $\pm$ 0.15 MPa, representing a 9.1% improvement in R^2 and a reduction of 32.5% in RMSE as compared to the Ridge baseline model. The model demonstrated excellent predictive capability for CS with an R^2 of 0.894 and a good performance for FS with an R^2 of 0.828, while showing moderate performance for STS with an R^2 of 0.537 due to the limited sample size (n = 159) and inherent variability of tensile testing. The experimental validation using wood waste biochar confirmed that model predictions closely matched measured strengths.
2. SHAP analysis identified cement content, CA content, and biochar dosage as the most influential features. Cement content showed a strong positive relationship with all strengths, while water-to-binder ratio exhibited a negative relationship consistent with Abrams' law. Biochar dosage displayed a non-linear pattern, with moderate dosages of 10 to 30 kg/m^3 increasing the CS, FS and STS.
3. Biochar effect curves, based on the most reliable datasets (rice husk, n = 69; wood, n = 52), demonstrated that rice husk biochar consistently enhanced all three strength properties, while wood biochar showed superior performance for FS and STS, consistent with the experimental results. Similarly, both experimental and modeling results confirmed optimal dosage ranges of 15–30 kg/m^3 for CS, 20 to 40 kg/m^3 for FS, and 10 to 20 kg/m^3 for STS.
4. The Pareto front analysis for optimizing the mix design revealed that low-cement mixes with cement content less than 350 kg/m^3 can achieve 35 to 45 MPa CS with 15 to 30 kg/m^3 biochar addition, representing optimal trade-offs between structural performance and environmental impacts.
5. The quantile regression models produced well-calibrated 90% prediction intervals, capturing 100% of experimental strength values at 28 days, confirming the practical utility of the uncertainty quantification approach.

The long-term performance studies are required to evaluate durability. Perform field validation studies using real-world construction conditions. Develop a user-friendly graphical interface with input validation, uncertainty visualization, and sensitivity analysis. Investigate wood biochar from diverse waste streams to assess variability in performance. Extend the predictive framework to include durability indicators. Also, integrate life cycle assessment with the predictive models to quantify environmental benefits.

5. Limitations

The dataset collected from different studies was not produced under identical experimental conditions and has variability from biochar feedstocks, particle sizes, pyrolysis temperatures, mix proportions, curing ages, and testing protocols. This heterogeneity is a limitation, but it also increases the diversity of the dataset and improves the model's ability to learn across a wider biochar-concrete design space. The dataset exhibits size disparity across target variables, with CS data available for all 318 samples, while FS and STS have the data available for 126 and 159 samples, respectively. Biochar type representation is uneven, with rice husk (n = 69) and wood (n = 52) dominating, while soybean dregs (n = 12) and olive pits (n = 9) are underrepresented. Dosage range limitations for several feedstocks (wood, maximum 37 kg/m^3, olive pits, maximum 24 kg/m^3) mean that predictions beyond these maxima are extrapolations. The substantial gap between training (R^2 = 0.960) and testing (R^2 = 0.544) performance for STS is attributed to the limited sample size and inherent variability of STS. This could also be attributed to the complex nature of biochar effects on tensile strength properties of concrete mixes. Similarly, STS is more sensitive to specimen preparation, loading alignment, crack initiation, interfacial transition zone behavior, and microstructural variability. The strength features in the data set included strength values from 3 to 90 days; however, in experimental work, 7-and 28-day testing is carried out.

Author Contributions: Conceptualization, S.R. and A.B.-J.; methodology, S.R. and A.B.-J.; software, S.R. and A.B.-J.; validation, A.B.-J.; formal analysis, S.R.; investigation, S.R.; resources, S.R. and A.B.-J.; data curation, S.R.; writing—original draft preparation, S.R.; writing—review and editing, S.R., A.B.-J., M.A.T. and Z.T.; visualization, S.R. All authors have read and agreed to the published version of the manuscript.

Funding: This research received no external funding.

Institutional Review Board Statement: Not applicable.

Informed Consent Statement: Not applicable.

Data Availability Statement: The original contributions presented in this study are included in the article. Further inquiries can be directed to the corresponding author.

Conflicts of Interest: The authors declare no conflicts of interest.

References

1. Khankhaje, E.; Kim, T.; Jang, H.; Kim, C.; Kim, J.; Rafieizonooz, M. A review of utilization of industrial waste materials as cement replacement in pervious concrete: An alternative approach to sustainable pervious concrete production. *Heliyon* **2024**, *10*, e26188. [CrossRef] [PubMed]
2. Busch, P.; Kendall, A.; Murphy, C.W.; Miller, S.A. Literature review on policies to mitigate GHG emissions for cement and concrete. *Resour. Conserv. Recycl.* **2022**, *182*, 106278. [CrossRef]
3. Adesina, A. Recent advances in the concrete industry to reduce its carbon dioxide emissions. *Environ. Chall.* **2020**, *1*, 100004. [CrossRef]
4. Iqbal, S.; Zaheer, M.; Room, S. Mechanical & microstructural properties of self-compacting concrete by partial replacement of cement with marble powder and sand with rice husk ash. *Int. Q. Res. J.* **2023**, *4*, 82–99.
5. United Nations Environment Programme (UNEP). *2023 Global Status Report for Buildings and Construction: Beyond Foundations—Mainstreaming Sustainable Solutions to Cut Emissions from the Buildings Sector*; United Nations Environment Programme (UNEP): Nairobi, Kenya, 2024. [CrossRef]
6. Hafez, H.; Teirelbar, A.; Kurda, R.; Tošić, N.; de la Fuente, A. Pre-bcc: A novel integrated machine learning framework for predicting mechanical and durability properties of blended cement concrete. *Constr. Build. Mater.* **2022**, *352*, 129019. [CrossRef]
7. Room, S.; Bahadori-Jahromi, A. Hydration Kinetics of Biochar-Enhanced Cement Composites: A Mini-Review. *Buildings* **2025**, *15*, 2520. [CrossRef]

8. Valpak Consulting; Verde Research & Consulting; WRAP. *Wood Flow 2025—Wood Packaging Flow Data Report*; WRAP (Waste & Resources Action Programme): London, UK, 2020. Available online: https://www.wrap.ngo/resources/report/wood-flow-2025-wood-packaging-flow-data-report (accessed on 10 February 2026).
9. Westbury, P.; Arlinghaus, J.; Bateman, I.; Beerling, D.; Bellamy, R.; Brophy, A.; Butnar, I.; Donnison, I.; Evans, C.; Gilbert, A.; et al. *The UKRI Strategic Priorities Fund Greenhouse Gas Removal Demonstrators (GGR-D) Programme: An Overview of Key Research Insights and Cross-Cutting Lessons*; Grantham Institute for Climate Change: London, UK, 2025. [CrossRef]
10. Department for Business, Energy & Industrial Strategy (BEIS). Net Zero Strategy: Build Back Greener. 2021. Available online: https://www.gov.uk/government/publications/net-zero-strategy (accessed on 10 February 2026).
11. Room, S.; Bahadori-Jahromi, A. Biochar-Enhanced Carbon-Negative and Sustainable Cement Composites: A Scientometric Review. *Sustainability* **2024**, *16*, 10162. [CrossRef]
12. Gupta, S.; Kua, H.W.; Low, C.Y. Use of biochar as carbon sequestering additive in cement mortar. *Cem. Concr. Compos.* **2018**, *87*, 110–129. [CrossRef]
13. Wang, L.; Chen, L.; Tsang, D.C.W.; Kua, H.W.; Yang, J.; Ok, Y.S.; Ding, S.; Hou, D.; Poon, C.S. The roles of biochar as green admixture for sediment-based construction products. *Cem. Concr. Compos.* **2019**, *104*, 103348. [CrossRef]
14. Chen, T.; Yang, Z.; Liu, H.; Li, L.; Qin, L.; Gao, X. Effect of biochar characteristics on freeze-thaw durability of biochar-cement composites. *J. Build. Eng.* **2025**, *102*, 111959. [CrossRef]
15. Ling, Y.; Wu, X.; Tan, K.; Zou, Z. Effect of Biochar Dosage and Fineness on the Mechanical Properties and Durability of Concrete. *Materials* **2023**, *16*, 2809. [CrossRef] [PubMed]
16. Wang, D.; Sas, G.; Das, O. The importance of volumetric w/c for porous supplementary cementitious materials in concrete. *J. Build. Eng.* **2025**, *111*, 113290. [CrossRef]
17. Akhtar, A.; Sarmah, A.K. Novel biochar-concrete composites: Manufacturing, characterization and evaluation of the mechanical properties. *Sci. Total Environ.* **2018**, *616–617*, 408–416. [CrossRef]
18. Hussain, F.; Soliman, N. Explainable machine learning driven predictive modeling of biochar-based cementitious composite. *J. Build. Eng.* **2025**, *113*, 113942. [CrossRef]
19. Aslam, F.; Shahab, M.Z. Supplementary cementitious materials in blended cement concrete: Advancements in predicting compressive strength through machine learning. *Mater. Today Commun.* **2024**, *38*, 107725. [CrossRef]
20. Naseri, H.; Jahanbakhsh, H.; Hosseini, P.; Moghadas Nejad, F. Designing sustainable concrete mixture by developing a new machine learning technique. *J. Clean. Prod.* **2020**, *258*, 120578. [CrossRef]
21. Ziolkowski, P.; Niedostatkiewicz, M. Machine Learning Techniques in Concrete Mix Design. *Materials* **2019**, *12*, 1256. [CrossRef] [PubMed]
22. Salami, B.A.; Olayiwola, T.; Oyehan, T.A.; Raji, I.A. Data-driven model for ternary-blend concrete compressive strength prediction using machine learning approach. *Constr. Build. Mater.* **2021**, *301*, 124152. [CrossRef]
23. Amin, M.N.; Ahmad, W.; Khan, K.; Nazar, S.; Arab, A.M.A.; Deifalla, A.F. Evaluating the relevance of eggshell and glass powder for cement-based materials using machine learning and SHapley Additive exPlanations (SHAP) analysis. *Case Stud. Constr. Mater.* **2023**, *19*, e02278. [CrossRef]
24. Farooq, F.; Nasir Amin, M.; Khan, K.; Rehan Sadiq, M.; Faisal Javed, M.; Aslam, F.; Alyousef, R. A Comparative Study of Random Forest and Genetic Engineering Programming for the Prediction of Compressive Strength of High Strength Concrete (HSC). *Appl. Sci.* **2020**, *10*, 7330. [CrossRef]
25. Haque, M.E.; Arifuzzaman, M.; Khan, K.; Azad, A.K.M.; Alluqmani, A.E.; Kashem, A. Machine learning models for mechanical properties prediction of basalt fiber-reinforced concrete incorporating graphical user interface. *Sci. Rep.* **2025**, *15*, 37029. [CrossRef]
26. Jatti, V.S.; Saiyathibrahim, A.; Yadav, A.; R., M.K.; Jayaprakash, B.; Kaushal, S.; Jatti, V.S.; Jatti, A.V.; Jatti, S.V.; Kumar, A.; et al. Predicting the tensile properties of heat treated and non-heat treated LPBFed AlSi10Mg alloy using machine learning regression algorithms. *PLoS ONE* **2025**, *20*, e0324049. [CrossRef]
27. Manan, A.; Pu, Z.; Majdi, A.; Alattyih, W.; Elagan, S.K.; Ahmad, J. Sustainable optimization of concrete strength properties using artificial neural networks: A focus on mechanical performance. *Mater. Res. Express* **2025**, *12*, 025504. [CrossRef]
28. Kulasooriya, W.K.V.J.B.; Ranasinghe, R.S.S.; Perera, U.S.; Thisovithan, P.; Ekanayake, I.U.; Meddage, D.P.P. Modeling strength characteristics of basalt fiber reinforced concrete using multiple explainable machine learning with a graphical user interface. *Sci. Rep.* **2023**, *13*, 13138. [CrossRef] [PubMed]
29. Javed, M.F.; Khan, M.; Fawad, M.; Alabduljabbar, H.; Najeh, T.; Gamil, Y. Comparative analysis of various machine learning algorithms to predict strength properties of sustainable green concrete containing waste foundry sand. *Sci. Rep.* **2024**, *14*, 14617. [CrossRef]
30. Qing, S.; Li, C. Data-driven prediction on critical mechanical properties of engineered cementitious composites based on machine learning. *Sci. Rep.* **2024**, *14*, 15322. [CrossRef] [PubMed]
31. Zhou, Z.; Chakma, J.; Hoque, M.A.; Chakma, V.; Ahmed, A. Prediction of UHPC mechanical properties using optimized hybrid machine learning model with robust sensitivity and uncertainty analysis. *Mater. Res. Express* **2025**, *12*, 085703. [CrossRef]

32. Liu, J.; Han, X.; Pan, Y.; Cui, K.; Xiao, Q. Physics-assisted machine learning methods for predicting the splitting tensile strength of recycled aggregate concrete. *Sci. Rep.* **2023**, *13*, 9078. [CrossRef]
33. Wu, Y.; Cai, D.; Gu, S.; Jiang, N.; Li, S. Compressive strength prediction of sleeve grouting materials in prefabricated structures using hybrid optimized XGBoost models. *Constr. Build. Mater.* **2025**, *476*, 141319. [CrossRef]
34. *BS EN 197-1:2011*; Cement—Composition, Specifications and Conformity Criteria for Common Cements. British Standards Institution: London, UK, 2011.
35. *BS EN 12620:2013*; Aggregates for Concrete. British Standards Institution: London, UK, 2013.
36. *BS EN 934-2:2019*; Admixtures for Concrete, Mortar, and Grout—Part 2: Concrete Admixtures—Specifications. British Standards Institution (BSI): London, UK, 2019.
37. *BS 8500-1:2015*; Concrete—Complementary British Standard to BS EN 206—Part 1: Method of Specifying and Guidance for the Specifier. British Standards Institution: London, UK, 2015.
38. *BS 8500-2:2015*; Concrete—Complementary British Standard to BS EN 206—Part 2: Specification for Constituent Materials and Concrete Production. British Standards Institution (BSI): London, UK, 2015.
39. *BS EN 206:2013+A2:2021*; Concrete: Specification, Performance, Production and Conformity. British Standards Institution (BSI): London, UK, 2021.
40. Sirico, A.; Bernardi, P.; Sciancalepore, C.; Vecchi, F.; Malcevschi, A.; Belletti, B.; Milanese, D. Biochar from wood waste as additive for structural concrete. *Constr. Build. Mater.* **2021**, *303*, 124500. [CrossRef]
41. *BS EN 12350-2:2019*; Testing Fresh Concrete—Part 2: Slump Test. British Standards Institution: London, UK, 2019. Available online: https://knowledge.bsigroup.com/products/testing-fresh-concrete-slump-test-2 (accessed on 20 January 2026).
42. *BS EN 12350-6:2019*; Testing Fresh Concrete—Part 6: Density. British Standards Institution: London, UK, 2019.
43. *ASTM C138/C138M-24a*; Standard Test Method for Density (Unit Weight), Yield, and Air Content (Gravimetric) of Concrete. ASTM International: West Conshohocken, PA, USA, 2024.
44. *BS EN 12390-3:2019*; Testing Hardened Concrete—Part 3: Compressive Strength of Test Specimens. British Standards Institution: London, UK, 2019.
45. *BS EN 12390-6:2023*; Testing Hardened Concrete—Tensile Splitting Strength of Test Specimens. British Standards Institution (BSI): London, UK, 2023.
46. *BS EN 12390-5:2019*; Testing Hardened Concrete—Flexural Strength of Test Specimens. British Standards Institution (BSI): London, UK, 2019.
47. Nassar, R.; Room, S. Strength, Durability, and Microstructural Characteristics of Binary Concrete Mixes Developed with Ultrafine Rice Husk Ash as Partial Substitution of Binder. *Civ. Eng. Archit.* **2025**, *13*, 595–611. [CrossRef]
48. Thakur, A.; Agarwal, R.; Kumar, R.; Singh, S.; Athar, H.; Naik Banavath, S.; Sharma, M.; Rai, D. Enhancement of Concrete Performance and Sustainability through Partial Cement Replacement with Biochar: An Experimental Study. *Iran. J. Sci. Technol. Trans. Civ. Eng.* **2025**, *49*, 3549–3569. [CrossRef]
49. Zareei, S.A.; Ameri, F.; Dorostkar, F.; Ahmadi, M. Rice husk ash as a partial replacement of cement in high strength concrete containing micro silica: Evaluating durability and mechanical properties. *Case Stud. Constr. Mater.* **2017**, *7*, 73–81. [CrossRef]
50. Mahmoud, A.A.; El-Sayed, A.; Fathy, I.N.; Fawzy, S.; Alturki, M.; Elfakharany, M.E.; Abouelnour, M.A.; Mahmoud, K.A.; Dahish, H.A.; ElTalawy, S.M.; et al. Evaluation of rice husk biochar influence as a partial cement replacement material on the physical, mechanical, microstructural, and radiation shielding properties of ordinary concrete. *Sci. Rep.* **2025**, *15*, 27229. [CrossRef] [PubMed]
51. Ahmad, W.; Veeraghantla, V.S.; Byrne, A. Advancing Sustainable Concrete Using Biochar: Experimental and Modelling Study for Mechanical Strength Evaluation. *Sustainability* **2025**, *17*, 2516. [CrossRef]
52. Gupta, S.; Kua, H.W.; Pang, S.D. Effect of biochar on mechanical and permeability properties of concrete exposed to elevated temperature. *Constr. Build. Mater.* **2020**, *234*, 117338. [CrossRef]
53. Pang, X.; Qin, Y.; Wei, P.; Huang, C. Enhancing fire resistance: Investigating mechanical properties of biochar-infused concrete under elevated temperatures. *Constr. Build. Mater.* **2024**, *435*, 136813. [CrossRef]
54. Liu, H.; Li, Q. Preparation of green concrete from bamboo biochar (BB) and concrete slurry waste (CSW): Preparation method and performance evaluation. *Constr. Build. Mater.* **2025**, *462*, 139964. [CrossRef]
55. Revathi, S.; Alice Elizabeth Tania, D.; Ancy Shadin, S.; Keerthana, J. Effect of zeolite and bamboo biochar as CO_2 absorbant in concrete. *Carbon Res.* **2024**, *3*, 43. [CrossRef]
56. Coelho, N.P.F.; Nalon, G.H.; Mendes, J.F.; de Oliveira, T.J.P.; Mendes, R.F. Effects of coffee husk biochar on the properties of concrete. *Constr. Build. Mater.* **2025**, *491*, 142680. [CrossRef]
57. Beskopylny, A.N.; Stel'makh, S.A.; Shcherban', E.M.; Mailyan, L.R.; Meskhi, B.; Smolyanichenko, A.S.; Beskopylny, N. High-Performance Concrete Nanomodified with Recycled Rice Straw Biochar. *Appl. Sci.* **2022**, *12*, 5480. [CrossRef]
58. Ying, X.; Zhao, X.; Ye, M.; Wang, C.; Zhan, B.; Zhao, J.; He, Z.; Nie, X. Waste rice straw biochar recycled concrete: Carbon sequestration, durability and microstructure. *J. Clean. Prod.* **2025**, *512*, 145690. [CrossRef]

59. Liu, S.; Chen, Z.; Shao, J.; Luo, S.; Yu, D. Novel soybean dregs biochar concrete: Characterization and evaluation of the mechanical properties and microstructure. *Constr. Build. Mater.* **2025**, *458*, 139512. [CrossRef]
60. Li, Z.; Xue, W.; Zhou, W. Mechanical Properties of Concrete with Different Carya Cathayensis Peel Biochar Additions. *Sustainability* **2023**, *15*, 4874. [CrossRef]
61. Jia, Y.; Li, H.; He, X.; Li, P.; Wang, Z. Effect of biochar from municipal solid waste on mechanical and freeze–thaw properties of concrete. *Constr. Build. Mater.* **2023**, *368*, 130374. [CrossRef]
62. Nazar, S.; Yang, J.; Wang, X.; Khan, K.; Amin, M.N.; Javed, M.F.; Althoey, F.; Ali, M. Estimation of strength, rheological parameters, and impact of raw constituents of alkali-activated mortar using machine learning and SHapely Additive exPlanations (SHAP). *Constr. Build. Mater.* **2023**, *377*, 131014. [CrossRef]
63. Kashem, A.; Karim, R.; Malo, S.C.; Das, P.; Datta, S.D.; Alharthai, M. Hybrid data-driven approaches to predicting the compressive strength of ultra-high-performance concrete using SHAP and PDP analyses. *Case Stud. Constr. Mater.* **2024**, *20*, e02991. [CrossRef]
64. Borchani, H.; Varando, G.; Bielza, C.; Larrañaga, P. A survey on multi-output regression. *WIREs Data Min. Knowl. Discov.* **2015**, *5*, 216–233. [CrossRef]
65. Varma, S.; Simon, R. Bias in error estimation when using cross-validation for model selection. *BMC Bioinform.* **2006**, *7*, 91. [CrossRef]
66. Bahadori-Jahromi, A.; Room, S.; Paknahad, C.; Altekreeti, M.; Tariq, Z.; Tahayori, H. The Role of Artificial Intelligence and Machine Learning in Advancing Civil Engineering: A Comprehensive Review. *Appl. Sci.* **2025**, *15*, 10499. [CrossRef]
67. Gupta, S.; Kua, H.W.; Koh, H.J. Application of biochar from food and wood waste as green admixture for cement mortar. *Sci. Total Environ.* **2018**, *619–620*, 419–435. [CrossRef]
68. Sirico, A.; Belletti, B.; Bernardi, P.; Malcevschi, A.; Pagliari, F.; Fornoni, P.; Moretti, E. Effects of biochar addition on long-term behavior of concrete. *Theor. Appl. Fract. Mech.* **2022**, *122*, 103626. [CrossRef]
69. Maljaee, H.; Madadi, R.; Paiva, H.; Tarelho, L.; Ferreira, V.M. Incorporation of biochar in cementitious materials: A roadmap of biochar selection. *Constr. Build. Mater.* **2021**, *283*, 122757. [CrossRef]
70. Praneeth, S.; Guo, R.; Wang, T.; Dubey, B.K.; Sarmah, A.K. Accelerated carbonation of biochar reinforced cement-fly ash composites: Enhancing and sequestering CO_2 in building materials. *Constr. Build. Mater.* **2020**, *244*, 118363. [CrossRef]
71. Murali, G.; Wong, L.S. A comprehensive review of biochar-modified concrete: Mechanical performance and microstructural insights. *Constr. Build. Mater.* **2024**, *425*, 135986. [CrossRef]
72. Asadi Zeidabadi, Z.; Bakhtiari, S.; Abbaslou, H.; Ghanizadeh, A.R. Synthesis, characterization and evaluation of biochar from agricultural waste biomass for use in building materials. *Constr. Build. Mater.* **2018**, *181*, 301–308. [CrossRef]
73. Chen, Y.; Zou, Z.; Jin, X.; Wang, J.; Tan, K. Biochar-enhanced concrete mixes: Pioneering multi-objective optimization. *J. Build. Eng.* **2024**, *88*, 109263. [CrossRef]
74. Neville, A.M. *Properties of Concrete*, 5th ed.; Pearson Education Limited: Harlow, UK, 2011.
75. Cui, D.; Wang, L.; Zhang, C.; Xue, H.; Gao, D.; Chen, F. Dynamic Splitting Performance and Energy Dissipation of Fiber-Reinforced Concrete under Impact Loading. *Materials* **2024**, *17*, 421. [CrossRef]